The somatodendritic endosomal regulator NEEP21 facilitates axonal targeting of L1/NgCAM

Chan Choo Yap,[1] Dolora Wisco,[1] Pekka Kujala,[3,4] Zofia M. Lasiecka,[1] Johanna T. Cannon,[1] Michael C. Chang,[1] Harald Hirling,[2] Judith Klumperman,[3,4] and Bettina Winckler[1]

[1]Department of Neuroscience, University of Virginia Medical School, Charlottesville, VA 22908
[2]Brain Mind Institute, Ecole Polytechnique Federale de Lausanne, CH-1015 Lausanne, Switzerland
[3]Department of Cell Biology and [4]Institute for Biomembranes and Center for Biomedical Genetics, University Medical Center, University of Utrecht, 3584CX Utrecht, Netherlands

Correct targeting of proteins to axons and dendrites is crucial for neuronal function. We showed previously that axonal accumulation of the cell adhesion molecule L1/neuron-glia cell adhesion molecule (NgCAM) depends on endocytosis (Wisco, D., E.D. Anderson, M.C. Chang, C. Norden, T. Boiko, H. Folsch, and B. Winckler. 2003. *J. Cell Biol.* 162:1317–1328). Two endocytosis-dependent pathways to the axon have been proposed: transcytosis and selective retrieval/retention. We show here that axonal accumulation of L1/NgCAM occurs via nondegradative somatodendritic endosomes and subsequent anterograde axonal transport, which is consistent with transcytosis. Additionally, we identify the neuronal-specific endosomal protein NEEP21 (neuron-enriched endosomal protein of 21 kD) as a regulator of L1/NgCAM sorting in somatodendritic endosomes. Down-regulation of NEEP21 leads to missorting of L1/NgCAM to the somatodendritic surface as well as to lysosomes. Importantly, the axonal accumulation of endogenous L1 in young neurons is also sensitive to NEEP21 depletion. We propose that small endosomal carriers derived from somatodendritic recycling endosomes can serve to redistribute a distinct set of membrane proteins from dendrites to axons.

Introduction

Many of the diverse functions of neurons are regulated by endocytosis (Cremona and De Camilli, 1997; Alberts and Galli, 2003; for review see Garrido et al., 2003; Sudhof, 2004; for review see Winckler, 2004; Deinhardt and Schiavo, 2005; for review see Kennedy and Ehlers, 2006; Lai and Jan, 2006). Neurons elaborate a much more complex and diversified endosomal system than nonpolarized cells (Sachse et al., 2002). For instance, somatodendritic endosomes play crucial roles in synaptic function (for review see Kennedy and Ehlers, 2006). Distinct axonal endosomes are responsible for retrograde signaling from the nerve terminal (Susalka and Pfister, 2000; Segal, 2003; Howe and Mobley, 2004; Deinhardt and Schiavo, 2005), transport of degradative cargo, and local recycling at axonal growth cones (Kamiguchi and Lemmon, 2000; Alberts and Galli, 2003) and synapses (Slepnev and De Camilli, 2000; Schweizer and Ryan, 2006). The overwhelming majority of endosomal cargos that travel via fast axonal transport in the axon do so in a retrograde direction (Parton et al., 1992). Their final destinations can be degradative compartments in the soma, nondegradative "signaling endosomes," or transneuronal traffic to another neuron. However, long-range anterograde traffic of endosomes along axons is not usually observed but would be predicted to occur for cargos that transcytose from the dendrites to axons (von Bartheld, 2004; for review see Winckler, 2004).

Currently, the organization and regulation of these diverse endosomal routes is incompletely understood. Different compartments in the endosomal system can be distinguished by the content of their markers as well as by their morphology. Fig. 1 D depicts the basic organization of endosomes (Maxfield and McGraw, 2004). Three distinct pathways are indicated: the degradative pathway (Fig. 1 D, red arrows), the somatodendritic recycling pathway (green arrows), and the transcytotic pathway (blue arrows). In epithelial cells, recycling takes place from the early endosome (EE) or the recycling endosome (RE). By analogy, local recycling from somatodendritic EEs back to

Correspondence to B. Winckler: BWinckler@virginia.edu

P. Kujala's present address is the Dutch Cancer Institute, 1066 CX, Amsterdam, Netherlands.

Abbreviations used in this paper: A/D PI, axon-dendrite polarity index; AS-NEEP21, antisense NEEP21; DIV, day in vitro; EE, early endosome; LE, late endosome; MVB, multivesicular body; NEEP21, neuron-enriched endosomal protein of 21 kD; NgCAM, neuron-glia cell adhesion molecule; RE, recycling endosome; Tf, transferrin; TGN, trans-Golgi network; Ti-VAMP, toxin-insensitive vesicle-associated membrane protein.

The online version of this paper contains supplemental material.

The Journal of Cell Biology, Vol. 180, No. 4, February 25, 2008 827–842
http://www.jcb.org/cgi/doi/10.1083/jcb.200707143

the somatodendritic domain might also occur in neurons (Fig. 1 D, green arrow). Likewise, REs are capable of sorting cargos to distinct plasma membrane domains in polarized epithelial cells. In neurons, it is likely that the RE is also capable of polarized sorting of cargos toward multiple destinations, such as axons (Fig. 1 D, blue arrows) or dendrites (green arrows; Schmidt and Haucke, 2007).

Multiple proteins identified as regulators of endosomal traffic in nonneuronal cells are also important in neuronal endosomes (Alberts et al., 2003; Park et al., 2004; Brown et al., 2005; Deinhardt et al., 2006). Additionally, neuronal-specific endosomal proteins might carry out neuronal-specific functions. One such neuronal endosomal protein is the neuron-enriched endosomal protein of 21 kD (NEEP21). NEEP21 was identified as an interacting protein of the endosomal syntaxin 13 and localizes to rab4-positive, EEA1-negative EEs in PC12 cells (Steiner et al, 2002). NEEP21 plays a crucial role in regulating the trafficking of multiple receptors in neurons (Steiner et al., 2002, 2005; Debaigt et al., 2004; Alberi et al., 2005), including the synaptic trafficking of AMPA receptors during synaptic plasticity (Alberi et al., 2005; Steiner et al., 2005; Kulangara et al., 2007).

Several groups have investigated the mechanisms underlying axonal targeting of the neuron-glia cell adhesion molecule (NgCAM), the chick homologue of L1 (Kamiguchi and Lemmon, 1998; Burack et al., 2000; Sampo et al., 2003; Wisco et al., 2003; Chang et al., 2006; Boiko et al., 2007). Based in part on the undetectability of NgCAM in somatodendritic endosomes, one model proposed that NgCAM was sorted to the axon by selective axonal fusion independent of endocytosis (Sampo et al., 2003). In contrast, our own work did detect somatodendritic endocytosis of NgCAM (Wisco et al., 2003). In addition, inhibition of endocytosis greatly impaired axonal accumulation of NgCAM (Wisco et al., 2003). NgCAM therefore uses an endocytosis-dependent pathway to the axon. Whether a "selective fusion" pathway is operative for NgCAM in certain cell types or at certain developmental stages is still an open question.

The targeting of several other axonal proteins is also endocytosis dependent (Garrido et al., 2001; Sampo et al., 2003; Leterrier et al., 2006; Xu et al., 2006). Two endocytosis-dependent pathways to the axon have been proposed: transcytosis (Wisco et al., 2003) and selective retrieval/retention (Fache et al., 2004). In the transcytotic model, the protein is sorted in the trans-Golgi network (TGN) to the somatodendritic domain. After somatodendritic exocytosis, the protein is endocytosed into somatodendritic endosomes and trafficked to the axon from there. In the selective retrieval/retention model, no sorting occurs in the TGN but proteins are inserted uniformly in both somatodendritic and axonal domains. Preferential accumulation of the protein on the axonal surface then occurs by selectively removing it from the somatodendritic surface by endocytosis and degrading it. The axonal population, however, is selectively retained on the axonal plasma membrane (for reviews see Garrido et al., 2003; Winckler, 2004). The transcytotic model makes several specific predictions: endocytosed NgCAM enters EEs in the somatodendritic domain, sorts away from somatodendritically recycling transferrin (Tf), is not primarily degraded in lysosomes, travels anterogradely up the axon in endosomes, and ultimately recycles to the axonal surface (Fig. 1 D, blue). The selective retention/retrieval model, in contrast, predicts that NgCAM is primarily degraded in lysosomes after endocytosis, does not enter axons in endosomes, and does not recycle to the axonal surface (Fig. 1 D, red). These two pathway models can therefore be distinguished experimentally. In this work, we show that NgCAM accumulates on the axon by transcytosis rather than by selective retrieval/retention. We also show that NEEP21 function is required for efficient accumulation of NgCAM on the axon.

Results

Detectability of endocytosed NgCAM in somatodendritic endosomes depends on permeabilization conditions

Because it remains controversial whether or not NgCAM is found in somatodendritic endosomes (Sampo et al., 2003; Wisco et al., 2003), we first tested what variables might affect detection of endocytosed NgCAM in somatodendritic endosomes. Neither the transfection method nor the age of the culture showed any differences in the detectability of somatodendritic NgCAM endocytosis (Fig. S1 A, available at http://www.jcb.org/cgi/content/full/jcb.200707143/DC1). Detergent conditions, however, proved critical for reliable detection of endocytosed NgCAM (Fig. S1, B–E). The discrepancy between the findings of Sampo et al. (2003) and our own (Wisco et al., 2003) therefore likely reflects differences in permeabilization conditions. Similarly to NgCAM, human L1-myc (Fig. S1 F) and rat L1-myc (not depicted) were internalized into somatodendritic endosomes. Cross linking of NgCAM by divalent anti-NgCAM IgGs is not necessary for the detectability of NgCAM in somatodendritic endosomes because somatodendritic endocytosis can also be observed with comparable efficiency (i.e., 70–80% of cells) when anti-NgCAM Fab fragments are used for the endocytosis assay (Fig. S1 G).

Endocytosed NgCAM colocalizes with somatodendritic EEs and partially localizes with lysosomes

The selective retrieval/retention model predicts that endocytosed NgCAM would be primarily degraded (Fig.1 D, red), whereas the transcytotic model predicts that NgCAM would largely bypass the late endosome (LE)/lys (Fig. 1 D, blue). We, therefore, asked whether endocytosed NgCAM in the somatodendritic domain initially colocalized with a marker for EEs (EEA1), and whether or not it ultimately accumulated with a marker for LE/lys (lgp120; see Materials and Methods for details on quantification). After incubating NgCAM-expressing cells for 20 min with anti-NgCAM antibodies (t = 0), 55% of all labeled endosomes contained both endocytosed NgCAM and EEA1 (Fig. 1 C, yellow, orange, and light green segments on the left), 23% of all labeled endosomes contained only EEA1 (Fig. 1 A, red; and Fig. 1 C, left, red). If only EEA1-positive endosomes were analyzed, 71% of them contained some endocytosed NgCAM ("high" plus "low" colocalization categories). We currently do not know if the high and low colocalization endosomes represent functionally distinct endosomal populations but they might reflect progressive sorting of NgCAM out of EEA1-positive endosomes.

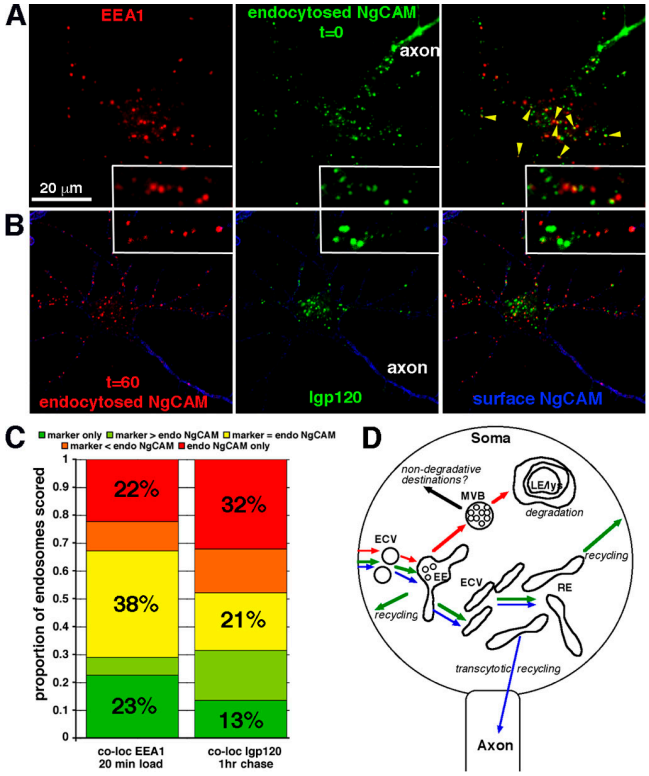

Figure 1. **Colocalization of endocytosed NgCAM with markers for early and late endosomes.** (A) NgCAM-expressing neurons were incubated for 20 min with anti-NgCAM antibodies, which were detected after permeabilization with an Alexa 488–goat anti–mouse antibody, whereas EEs were detected with a polyclonal anti-EEA1 antibody (red). Yellow arrowheads indicate examples of colocalizing puncta. (B) NgCAM-expressing neurons were incubated with anti-NgCAM antibody for 30 min at 16°C and washed, and internalized NgCAM antibody was chased at 37°C for 1 h. Surface NgCAM was detected before permeabilization with a cy5–goat anti–mouse secondary antibody (blue). After permeabilization, endocytosed NgCAM antibodies were detected with Alexa 568–goat anti–mouse antibody (red) and LEs/lysosomes were detected with a polyclonal anti-lgp120 antibody (green). A single confocal section is shown. The boxed regions shown in A and B are magnified sections of dendrites for easier comparison of colabeling. (C) Quantification of colocalization of EEA1 and NgCAM endocytosed for 20 min and of lgp120 and NgCAM endocytosed and chased for 60 min. For each puncta, the ratio of intensities of endocytosed NgCAM to either EEA1 (left) or lgp120 (right) was determined as described in Materials and methods. For EEA1 colocalization, 560 endosomes were scored. For lgp120 colocalization, 497 endosomes were scored. (D) Basic organization of endosomes, adapted from fibroblasts. Three distinct pathways are indicated by the arrows: degradative cargo follows the red arrows, somatodendritically recycling cargo follows the green arrows, and transcytosing cargo follows the blue arrows. Cargo enters via several pathways in small carriers vesicles (ECV) that fuse with existing EEs. EEs contain a vacuolar portion as well as tubular extensions. The tubular extensions accumulate recycling cargoes and bud off to transport recycling cargos back to the plasma membrane either directly or via the RE. Endosomal carrier vesicles (ECVs) can be spherical or elongated and serve as transport carriers between compartments. The vacuolar portions of the EE accumulate internal vesicles and mature into MVBs. MVBs are transport carriers that carry cargo to LE/lysosomes (LE/lys) for degradation (red). Some MVBs might not be predegradative but be capable of recycling. Cargo destined for either axons or dendrites are sorted in the RE and transported to their respective final destination from there.

Endocytosed NgCAM, which had been chased for 1 h (t = 60) to allow accumulation in a terminal compartment, colocalized partially with lgp120 (21% of all labeled endosomes; Fig. 1 B, yellow; and Fig. 1 C, right, yellow), whereas 32% contained only endocytosed NgCAM (Fig. 1, B and C, right, red). Of the somatic endosomes containing endocytosed NgCAM at long chase times, 47% also contained various amounts of lgp120. Because ~50% of endocytosed NgCAM leaves the somatodendritic endosomes in 90 min (see Fig. 3 B), we estimate that ~25% of endocytosed NgCAM ultimately accumulates in lysosomes. Because all proteins turn over to some degree at all times, some NgCAM is expected to localize to lysosomes. We note that complete quantification of NgCAM localization to lysosomes is not possible because some NgCAM and bound antibody might have been already degraded.

Somatodendritic endosomes contain endocytosed NgCAM by immuno-EM

Next, we sought to identify the somatic compartments containing NgCAM on the ultrastructural level. NgCAM at steady-state was found prominently in multivesicular bodies (MVBs; Fig. 2 A, asterisks) in the soma. Small profiles (Fig. 2 A, arrowheads) were also labeled. The exact identity of these compartments is not known but they might correspond to transport carriers or tubular portions of EEs.

To visualize endocytosed NgCAM, neurons were incubated simultaneously with an anti-NgCAM antibody and the fluid-phase marker gold-BSA and then processed for immuno-EM (Oorschot et al., 2002). Gold-BSA is ultimately transported to lysosomes and does not accumulate in REs. We therefore determined if endocytosed NgCAM could accumulate in compartments that exclude gold-BSA. Endocytosed NgCAM, detected by 15-nm gold-coupled protein A, was most often found in MVBs together with 3-nm gold-BSA (Fig. 2, B–D). Some of these NgCAM-positive MVBs contained no or very little gold-BSA (Fig. 2, C and D). 15 nm gold was also occasionally associated with tubules devoid of gold-BSA, which is reminiscent of recycling endosomal compartments (Fig. 2 E; Peden et al., 2004). NgCAM is therefore capable of entering nondegradative endosomal compartments including REs, but is also found in presumptive predegradative compartments.

Endocytosed NgCAM traverses somatodendritic endosomes and recycles preferentially to the axonal plasma membrane

The fate of endocytosed NgCAM was followed using a pulse-chase approach with an acid strip. We incubated NgCAM-expressing neurons with an anti-NgCAM antibody for 20 min (load) and then removed all remaining surface-bound antibody using an acid strip step. Cells were then returned to the incubator for various amounts of time (chase). After loading (t = 0), endocytosed NgCAM could be detected prominently in somatodendritic endosomes (Fig. 3 A) and was also seen, though less brightly, in endosomes along axons (Fig. 3 A, arrows). After 90 min of chase, the soma fluorescence was decreased (Fig. 3 B), whereas axonal endosomes were still bright (Fig. 3 B, arrows). Quantification of the soma-associated fluorescence showed that the half-time for depleting the soma signal was ~90 min (Fig. 3 C, open diamonds). Tf, however, disappeared from the soma with

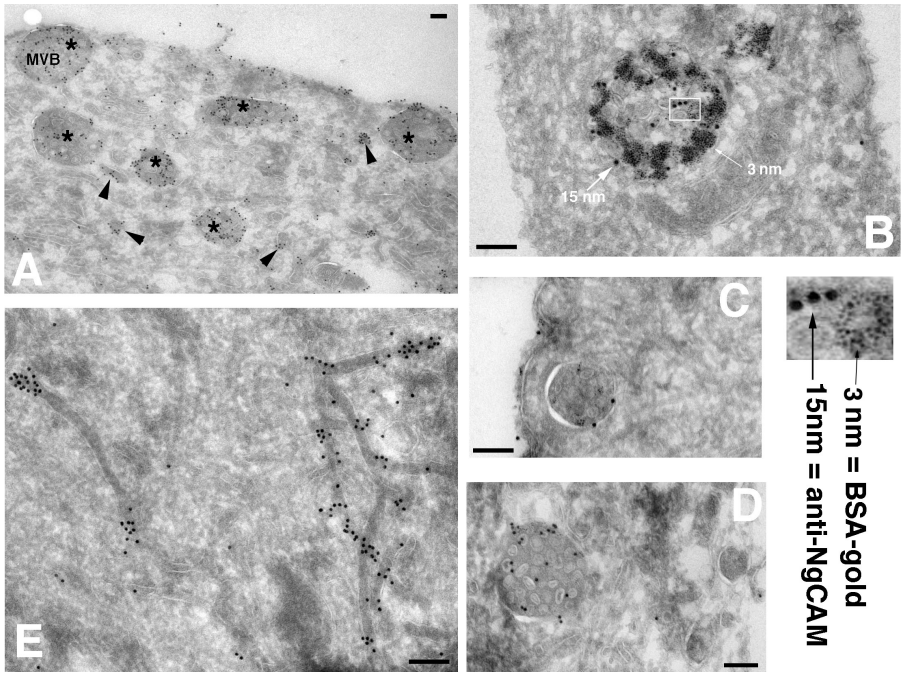

Figure 2. **Ultrastructural identification of NgCAM-containing somatic endosomes.** (A) Hippocampal neurons were infected with AdNgCAM for 24 h and subsequently fixed. NgCAM was detected with anti-NgCAM antibodies and 15 nm gold–protein A. NgCAM is found on the plasma membrane, in numerous MVBs (asterisks), and in small profiles of unknown identity (arrowheads). (B–E) NgCAM-expressing neurons were fed with anti-NgCAM antibodies and 3 nm gold-BSA for 15–60 min and then washed and fixed. Endocytosed NgCAM (15 nm gold) is found in MVBs together with varying amounts of 3 nm gold BSA. The labeled MVB in B contains many 3-nm gold particles (appearing as dark, grainy material) as well as large 15-nm gold particles (arrows). A larger magnification of the boxed region is shown in the inset below to highlight the two different sizes of particles. The MVB in C has few 3-nm gold particles, whereas the one in D has virtually none. (E) Occasionally, NgCAM is found in tubules that are devoid of cointernalized BSA-gold and likely represent RE. Bars, 150 nm.

a half-time of ∼25 min (Fig. 3 C, circles). To estimate the abundance of endocytosed NgCAM within dendritic and axonal endosomes, we quantified the intensity of individual endosomes in axons and dendrites. Endosomes correspond to the peaks in intensity line scans (Fig. 3 D) taken along dendrites and axons after the loading step (t = 0′) and at t = 90′. At t = 0, dendritic endosomes were on average about twofold brighter than axonal endosomes (Fig.3 D, top; axon/dendrite intensity ratio = 0.58). At t = 90′, axonal endosomes were on average 40% brighter than dendritic endosomes (Fig. 3 D bottom; axon/dendrite intensity ratio = 1.39). Endocytosed NgCAM, therefore, progressively disappeared from somatodendritic endosomes and accumulated in axonal endosomes.

To see if internalized NgCAM ever reappeared on the cell surface, we performed a load/acid strip/chase experiment as described in the previous paragraph but incubated the cells with Alexa 647–coupled secondary anti–mouse antibodies before permeabilization to stain the recycled surface pool (see Materials and methods). Initially, no surface labeling could be detected (Fig. 3 A′), but surface reappearance was easily detected at t = 90′ (Fig. 3 B′ and C, triangles and broken line). To determine to which surface endocytosed NgCAM recycled, we determined the axon-dendrite polarity index (A/D PI; see Materials and methods) for recycling NgCAM. At t = 40′, surface NgCAM staining already was threefold higher on the axonal surface. By t = 90′, it was 4.7-fold higher. By 2.5 h of chase, the recycling A/D PI was 5.5, the same as the steady-state A/D PI for NgCAM. NgCAM therefore recycled with at least a threefold bias toward the axon.

Endocytosed NgCAM accumulates in stationary somatodendritic endosomes and is transported in small endosomal carriers

We next imaged trafficking of endosomal NgCAM by feeding anti-NgCAM antibodies coupled to Alexa 488 to NgCAM-expressing neurons for 1 h in a live-imaging chamber. Cells were then washed and images were taken every 2 or 3 s for about 1 min. Endocytosed NgCAM was easily detected in somatodendritic endosomes in live cells (Fig. 4, A and A′). The extent of endosome motility was displayed by merging three video frames into one RGB image such that the first frame appeared red, the second green, and the third blue (Fig. 4, A and A′). Interestingly, the majority of the bright endosomes in the soma were stationary during the imaging duration (Fig. 4, A and A′; and Video 1, available at http://www.jcb.org/cgi/content/full/jcb.200707143/DC1). A subset of NgCAM-containing endosomes underwent movements (Fig. 4, A and A′, arrowheads). The labeling intensity of the endosomes usually correlated with size, such that the large stationary endosomes were brightly labeled but the small moving carriers were faint. We frequently observed short, wiggling excursions that did not result in long-distance translocation. We also observed longer-range transport events of small tubules (Fig. 4 B, arrows) or small circular compartments (Fig. 4 C, arrows). Movements were often intermittent with pauses of many seconds interspersed with periods of movement. Frequently, a small transport carrier initially appeared to emerge from, and ultimately disappear into, a larger stationary endosome. 91% of NgCAM-containing endosomes in the soma and dendrites appeared to be round or irregularly shaped, whereas 9% appeared to be elongated (n = 232; Fig. 4 E). The elongated carriers frequently appeared to be of varying width and intensity along their lengths (see Sonnichsen et al., 2000). 22% of all observed NgCAM endosomes underwent movement during the 1-min imaging periods. Of all the moving compartments, 84% appeared small (estimated diameter of ∼0.2 μm) and round, whereas 14% appeared elongated. Large (estimated diameter, >1 μm) and medium-sized (estimated diameter, ∼0.7 μm) round compartments rarely moved (Fig. 4 E, white and black bars). NgCAM therefore accumulates in stationary

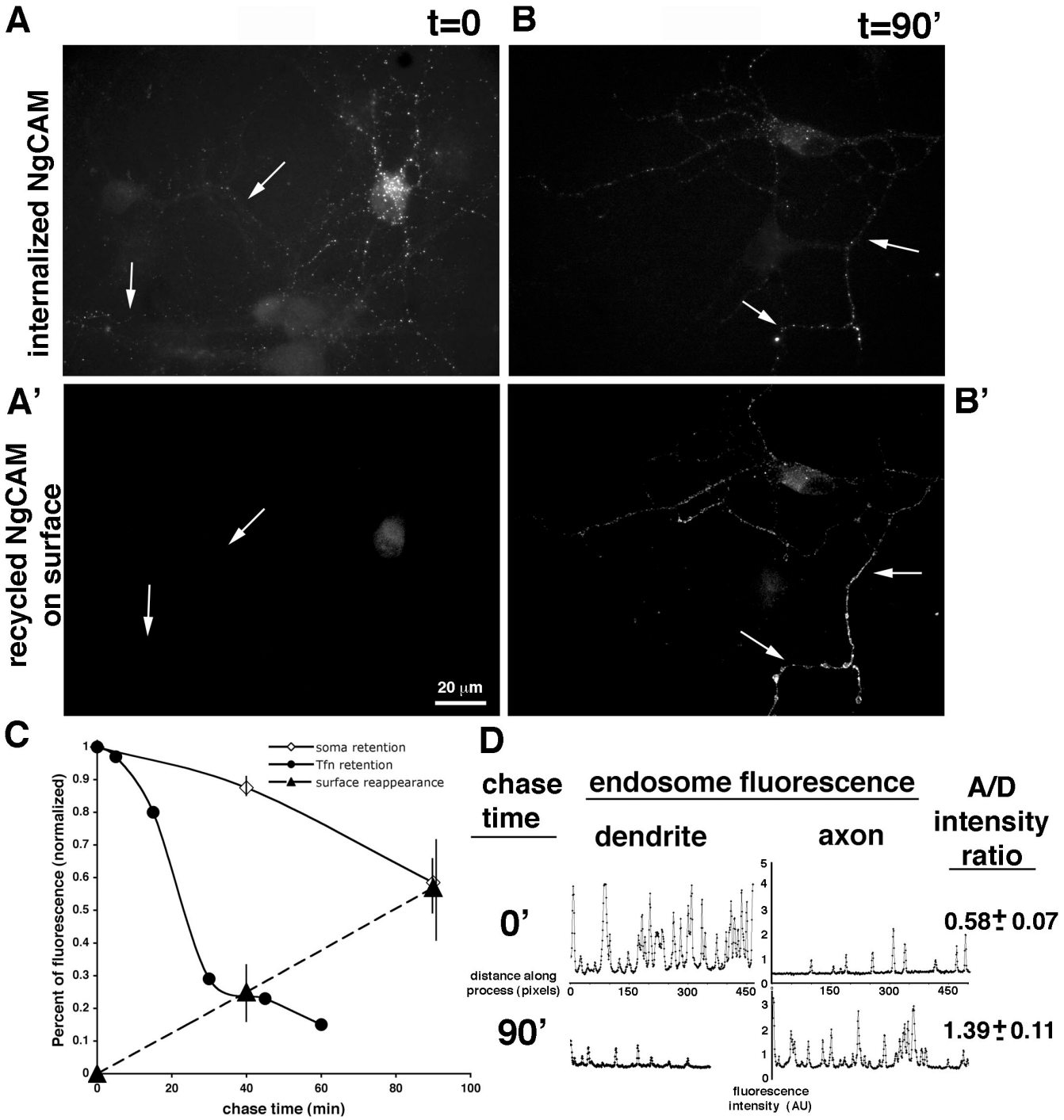

Figure 3. **Endocytosed NgCAM leaves somatic endosomes and recycles preferentially to the axonal plasma membrane.** (A) After 20 min of anti-NgCAM antibody loading (t = 0), intracellular endocytosed NgCAM can be visualized after acid stripping of surface-bound antibodies in somatodendritic but also axonal (arrows) endosomes. (B) After 90 min of chase at 37°C (t = 90′), somatodendritic endosomes are less prominently labeled, whereas axonal endosomes are still clearly detected (arrows). (A′ and B′) Surface reappearance of endocytosed NgCAM in the same cells was assayed with an Alexa 647–goat anti–mouse antibody after acid stripping and chase. No surface labeling was detectable at t = 0 (A′), demonstrating the efficiency of the acid strip. After 90 min of chase, axonal surface labeling was apparent (B′), demonstrating recycling of NgCAM to the plasma membrane. (C) The disappearance of somatic endosomal NgCAM was plotted as percentage of fluorescence remaining after acid stripping over time (open diamonds). Recycling of Tf from somatic endosomes was plotted as well (circles). Surface reappearance of endocytosed NgCAM was plotted as percentage of the chase end point of 2.5 h (triangles and broken line). The mean of four independent experiments is shown. SEM is indicated for each time point. (D) Representative intensity line scans are shown for dendrites at t = 0 (top left), axons at t = 0 (top right), dendrites at t = 90 min (bottom left), and axons at t = 90 min (bottom right). Brightly staining endosomes correspond to the peaks on the trace. The ratio of axon/dendrite average puncta intensity for t = 0 and t = 90 min is indicated to the right of the traces. *n* = 4 independent experiments.

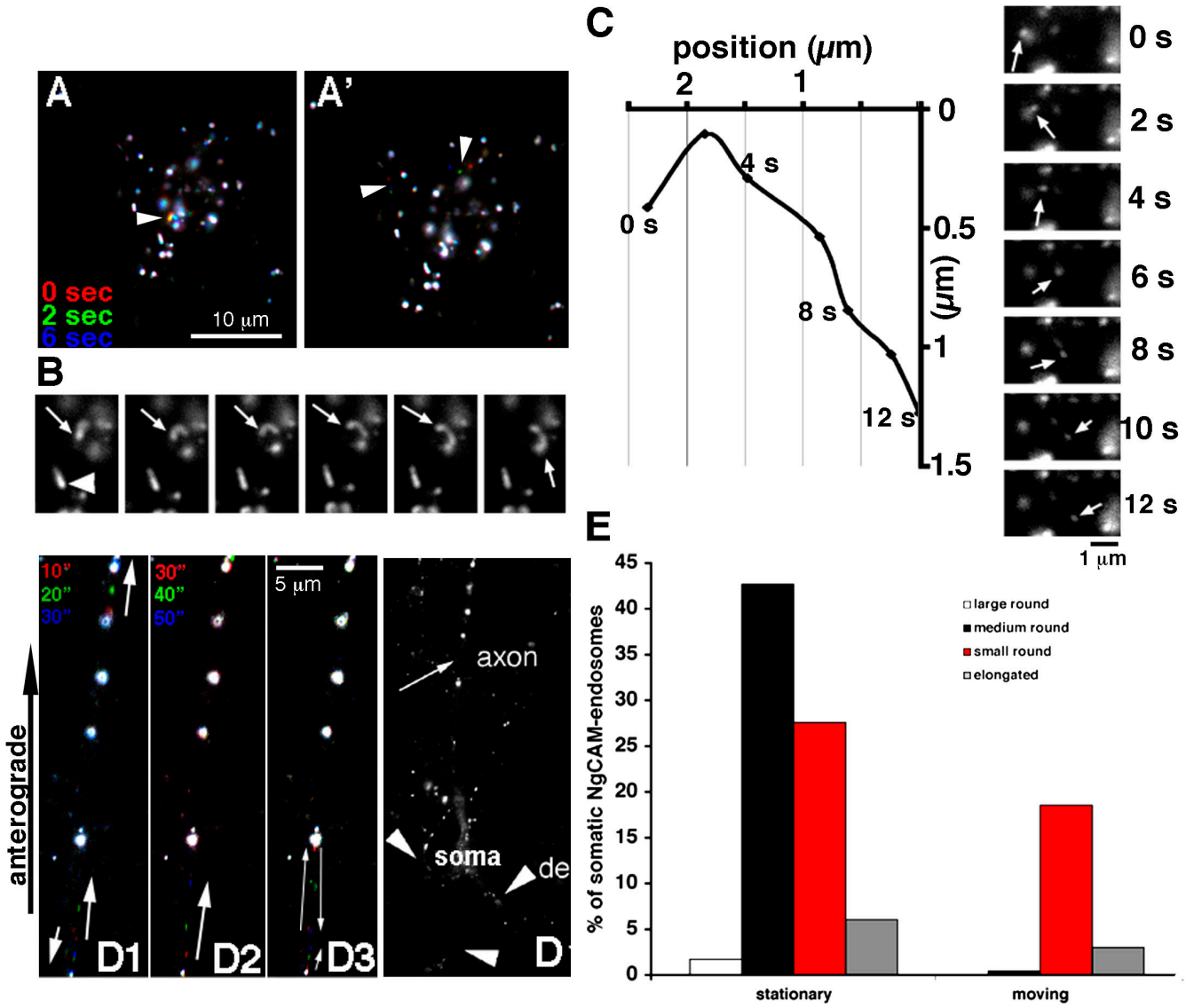

Figure 4. **Live imaging of NgCAM-containing endosomes.** (A–C) Neurons (DIV10) transfected with NgCAM were allowed to endocytose Alexa 488–anti-NgCAM antibodies in live imaging chambers for 60 min before washing and imaging at an acquisition speed of 0.5 Hz. Somatodendritic endosomes can be easily visualized (A and A'). See Video 1 (available at http://www.jcb.org/cgi/content/full/jcb.200707143/DC1). (A and A') Three frames of video were merged so that frame 1 (0 s) is red, frame 2 (2 s) is green, and frame 3 (6 s) is blue. Nonmoving endosomes therefore appear white. Moving endosomes appear colored (arrowheads). (B and C) Single frames of endocytosed NgCAM, 2 s apart, are shown to illustrate examples of a moving NgCAM-containing tubule (B, arrow), a nonmoving tubule (B, arrowhead), or a moving NgCAM-containing round carrier (C, arrow). The trajectory of the carrier in C is depicted on the graph. The speeds of observed movements ranged from 0.1 to 1.4 μm/s, averaging 0.5 μm/s. (D) Axonal endosomes were imaged live after acid stripping. A lower magnification image of the labeled cell is shown. Axons and dendrites are indicated with arrows and arrowheads, respectively. (D1–D3) Anterograde and retrograde movements of small NgCAM-containing endosomal carriers in the axon are observed (arrows). Three examples are shown in D1–D3, where frame 1 is red, frame 2 is green, and frame 3 is blue. Frames are 10 s apart as indicated (see Video 2). Nonmoving endosomes appear white. Anterograde movement is toward the top. Fig. S2 shows a single channel display. (E) Quantification of the behavior of NgCAM-containing somatodendritic endosomes. Three size classes are distinguishable: large round (apparent diameter, 1–1.3 μm), medium round (apparent diameter, 0.6–0.8 μm), small round (0.2–0.3 μm), and elongated. NgCAM was mostly transported in small round endosomal carriers. *n* = 232.

somatodendritic endosomes but is transported intermittently in small transport carriers.

Endocytosed NgCAM travels anterogradely in axons

Retrograde transport of endosomes has been well described (Overly and Hollenbeck, 1996; Segal, 2003; Deinhardt and Schiavo, 2005). Whether or not endosomal cargo travels anterogradely in axons has not been established. We therefore sought to determine the mobility of NgCAM endosomes in the axon (see Materials and methods). Again, most of the bright round endosomes containing NgCAM were not motile (Fig. 4, D1–D3, white puncta). Because the moving endosomal carriers are small and faint, imaging of axonal motile endosomes was technically challenging and extensive quantification proved not to be feasible. Nonetheless, we could observe clear examples of moving transport carriers containing endocytosed NgCAM (Fig. 4 D and Video 2, available at http://www.jcb.org/cgi/content/full/jcb.200707143/DC1)

in both the anterograde and retrograde direction (Fig. 4, D1–D3, arrows; and Video 2) with speeds ranging from 0.3 to 1.8 µm/s. Slightly more than half of the movements occurred in the anterograde direction. Therefore, small NgCAM-containing endosomal carriers travel up the axon by anterograde axonal transport, whereas large stationary endosomes in the axon accumulate endocytosed NgCAM. We do not currently know whether the retrogradely transported NgCAM is degraded in lysosomes or can recycle to the plasma membrane.

Endocytosed NgCAM transiently colocalizes with recycling Tf

Tf is a marker for the somatodendritic recycling pathway (Fig. 1 D, green; Hemar et al., 1997). The transcytotic model predicts that NgCAM initially internalizes into the same EE as Tf but ultimately sorts away from Tf into distinct endosomes and is sorted to axons from there. We incubated FITC-Tf–loaded cells with anti-NgCAM antibody at 16°C for 30 min to allow entry into the EE (Schmid and Smythe, 1991). Cells were then washed and incubated at 37°C in the continued presence of FITC-Tf for chase times of 5–120 min. At 5 min of NgCAM chase, NgCAM and Tf showed numerous clear examples of precise overlap (unpublished data), suggesting that NgCAM initially entered the Tf-containing EE, which is consistent with the colocalization of EEA1 and endocytosed NgCAM (Fig. 1 A). At 15 min of chase, we already observed many puncta containing only endocytosed NgCAM (Fig. 5 A, left, red). Because Tf was loaded to a steady state, these puncta correspond to a compartment in which Tf does not significantly accumulate. Precise colocalization of Tf and endocytosed NgCAM at 15 min of chase could also be observed (Fig. 5 A, arrowheads). After chase times of 60 min (Fig. 5 A, right), Tf- and NgCAM-positive regions frequently appeared closely apposed but not precisely overlapping. In these cases, the red and green channels were laterally offset, appearing as multicolored "traffic lights" (Fig. 5 A, right, arrowheads), which suggests that Tf and NgCAM largely occupied either distinct compartments or distinct domains of the same compartment (see also Thompson et al., 2007). This pattern of localization suggested that NgCAM and Tf entered the same EEA1-positive EE and subsequently sorted away from one another in a somatodendritic endosomal compartment, presumably an RE.

Dual live imaging of endocytosed NgCAM and Tf

We next imaged NgCAM-expressing cells loaded with Texas red–Tf and Alexa 488–coupled anti-NgCAM antibodies to see if Tf and NgCAM were transported together in endosomal carriers (see Materials and methods). The Tf-positive compartments correspond to REs because they still contained Tf after >20 min of chase. We observed somatodendritic endosomes containing both (Fig. 5, B and C, yellow), or either one of the cargos (Fig. 5, B and C, green and red). 42% of endosomes contained both NgCAM and Tf, 30% contained only NgCAM, and 28% contained only Tf (n = 365). Fig. 5 B demonstrates some of the classes of behaviors we observed: arrowheads designate some of the stationary endosomes, whereas arrows designate motile endosomes (Vidoes 3–6, available at http://www.jcb.org/cgi/content/full/jcb.200707143/DC1). Of all labeled endosomes (n = 365), 17% underwent movements in 50 s of imaging. Tf-containing compartments frequently wiggled about randomly, but only a few examples of rapid directed movement of Tf-containing compartments could be observed (Fig. 5 B, red arrow; and Fig. 5 D, right). Many of the compartments containing only Tf were large and pleiomorphic. Shape changes in these large structures did not permit quantification of individual compartments. In contrast, we frequently saw clear examples of mobile small spherical and tubular elements. These motile compartments tended to be largely devoid of Tf, with 70% of mobile compartments containing only NgCAM (Fig. 5 D, middle; and Video 3). Small spherical endosomes showed the most motility (Fig. 5 B, green arrow; Fig. 5 D, middle; and Video 4).

In addition, we observed red and green puncta that moved as a unit (Fig. 5 C and Video 5), which is reminiscent of the traffic light patterns observed in fixed samples (Fig. 5 A, right). These images might represent single membrane-bound elongated compartments in which Tf and NgCAM are laterally segregated. Such lateral segregation of cargos in REs is also found in other cell types, including MDCK cells (Thompson et al., 2007) and macrophages (Manderson et al., 2007). To visualize the laterally segregated cargos, a fluorescent lipid (DiIC18[5]-DS) was allowed to coendocytose. This assay enabled the observation of two differently labeled cargos encompassed in single DiI-labeled structures (Manderson et al., 2007). Even though this technique still relies on light microscopy, observation of such structures is consistent with the existence of single compartments with laterally segregated components. We adapted this assay, feeding Tf and anti-NgCAM antibody as well as DiI. Surprisingly, DiI labeled the NgCAM-containing endosomes much more reliably than it labeled Tf-containing endosomes (Fig. S3 A, available at http://www.jcb.org/cgi/content/full/jcb.200707143/DC1), which suggests that the lipid composition of NgCAM and Tf endosomes is not identical and that DiI partitions preferentially into a subset of endomembranes in neurons. We occasionally observed endosomes labeled by all three tracers (two to five per cell out of hundreds). Among the triple-labeled profiles, endosomes with laterally offset NgCAM and Tf staining seemingly encompassed by a single DiI-labeled profile were common (Fig. S3, B–D). Endocytosed NgCAM therefore was found together with Tf in stationary REs in the soma but it segregated away from Tf and moved over long distances in small spherical or tubular endosomal carriers largely devoid of Tf.

Axonal polarization of NgCAM is sensitive to interference with NEEP21 but not toxin-insensitive vesicle-associated membrane protein (Ti-VAMP)

In PC12 cells, two proteins affect the endosomal recycling of L1, the toxin-insensitive VAMP Ti-VAMP/VAMP7 (Martinez-Arca et al., 2001) and NEEP21 (Steiner et al., 2002). Ti-VAMP is found in both somatodendritic and axonal endosomes, whereas NEEP21 is found only in somatodendritic endosomes. We used two function-interfering constructs, Ti-VAMP-DN

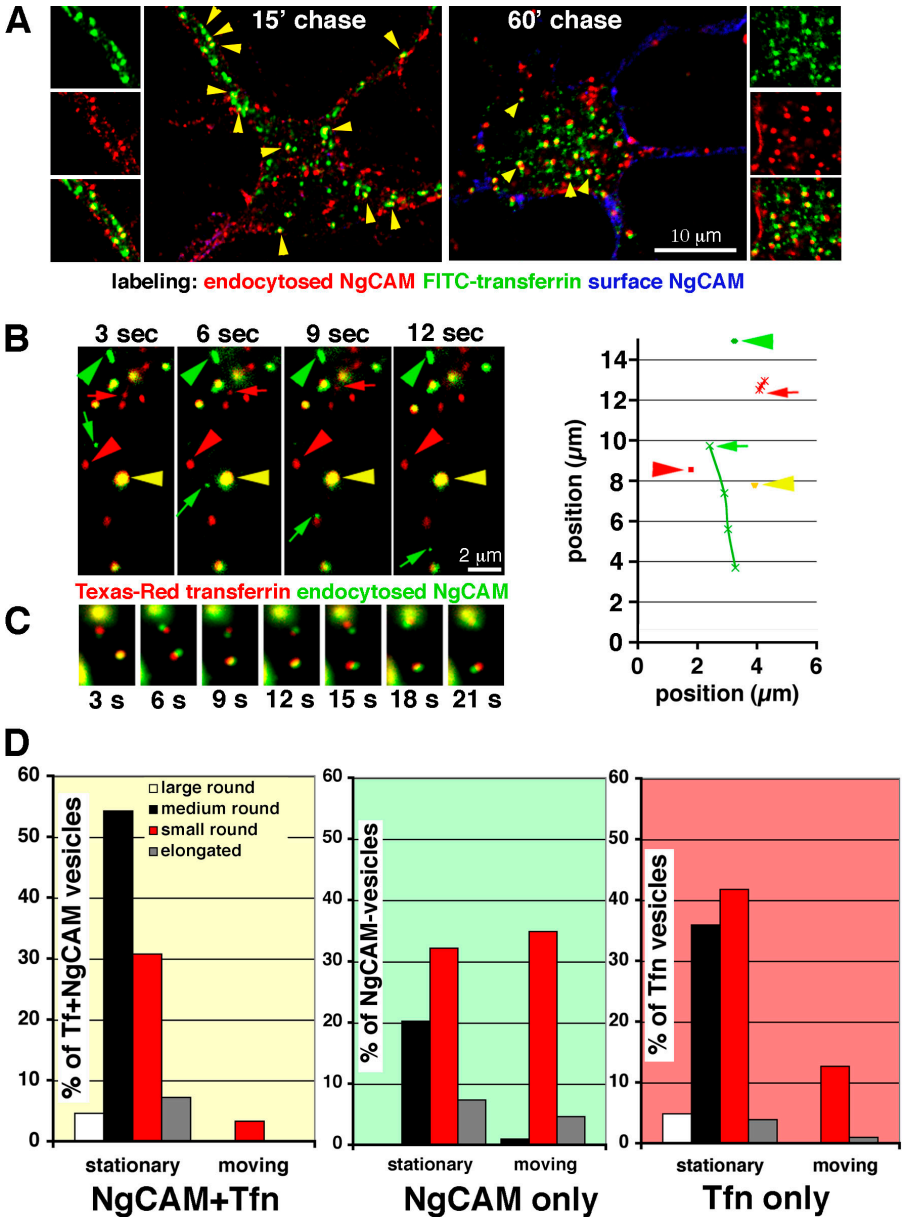

Figure 5. **Dual live imaging of internalized Tf and NgCAM.** (A) Neurons were transfected with NgCAM and incubated with anti-NgCAM antibodies (red) and FITC-Tf (green) at 16°C, washed and chased at 37°C in the continued presence of Tf for 15 (A, left) or 60 min (A, right), and then fixed. Surface NgCAM (blue) was detected with a cy5–anti–mouse secondary antibody before permeabilization. Yellow arrowheads indicate overlapping puncta. At 60 min of chase, the overlap is frequently not precise, resulting in a traffic light appearance. Single confocal sections are shown. The traffic light pattern is most abundant at late chase times. (B and C) Neurons (DIV12) expressing NgCAM were loaded with Texas red–Tf and Alexa 488–anti-NgCAM antibodies for 1 h and then washed and imaged live every 3 s. Tf (red) and endocytosed NgCAM (green) can be easily detected in somatodendritic endosomes in live neurons. See Video 3 (available at http://www.jcb.org/cgi/content/full/jcb.200707143/DC1). (B) Examples of endosome behavior is shown in four consecutive frames 3 s apart: stationary endosomes containing only NgCAM (green), only Tf (red), or both NgCAM and Tf (yellow) are indicated with arrowheads. Motile endosomal carriers are indicated by arrows (red, Tf only; green, NgCAM only). The four compartments marked with symbols were traced over time and their trajectories plotted in the adjacent graph. For the moving compartments, the arrow points at the first frame of the sequence. A proximal dendrite is shown. See Video 4. (C) Consecutive frames of a traffic light endosome are shown. The endosome appeared initially yellow but in subsequent frames appears as one slightly elongated carrier (or two tethered carriers) in which Tf (red) is laterally segregated away from endocytosed NgCAM (green). The field shown is from the soma of the cell. See Video 5. (D) Labeled endosomal puncta were categorized as Tf only, NgCAM only, or both NgCAM and Tf. All labeled structures in each panel were subdivided by shape (round or elongated) and size (large, medium, or small) and by motility (stationary or moving). Structures containing both Tf and NgCAM rarely moved, whereas structures containing Tf only moved occasionally. Structures containing NgCAM only were the most motile. *n* = 365 endosomes.

(Martinez-Arca et al., 2001) and antisense NEEP21-GFP (AS-NEEP21; see Materials and methods for details; Steiner et al., 2002). GFP was cotransfected with NgCAM as a control. Coexpression of Ti-VAMP-DN did not significantly affect A/D PI for NgCAM (Fig. 6 A, left), even though it profoundly inhibited axon outgrowth if introduced at day in vitro (DIV) 2 (not depicted; Martinez-Arca et al., 2001). Coexpression of AS-NEEP21, however, led to missorting of NgCAM to dendrites, resulting in a statistically significant reduction of NgCAM A/D PI (Fig. 6 A, right). NEEP21 is therefore a regulator of NgCAM transport in hippocampal neurons.

Endocytosed NgCAM (red) substantially and precisely overlapped with endogenous NEEP21 (Fig. 6 B, green) in somatodendritic endosomes (66% of all labeled endosomes; Fig. 6 C, left). Of NEEP21-containing endosomes, 86% contained endocytosed NgCAM at t = 0. At 1 h, the percentage of all labeled endosomes containing both NEEP21 and endocytosed NgCAM fell to 48% (Fig. 6 C, right). The NEEP21 compartment, therefore, behaves kinetically as an intermediate on the NgCAM pathway. Interestingly, the rate of clearance of endocytosed NgCAM from NEEP21 endosomes is slow, indicating that NgCAM has a long residence time in this compartment. Substantial colocalization with NEEP21 was also observed for endocytosed human and rat myc-L1 (not depicted). In contrast, NEEP21 (Fig. 6 D, green) showed only poor overlap with EEA1-positive EEs (red) in cultured hippocampal neurons (Fig. 6 D), as is the case in PC12 cells (Steiner et al., 2002).

Down-regulation of NEEP21 causes missorting of NgCAM in endosomes

Increased missorting to the somatodendritic domain could arise by several mechanisms. NgCAM might be expressed at higher

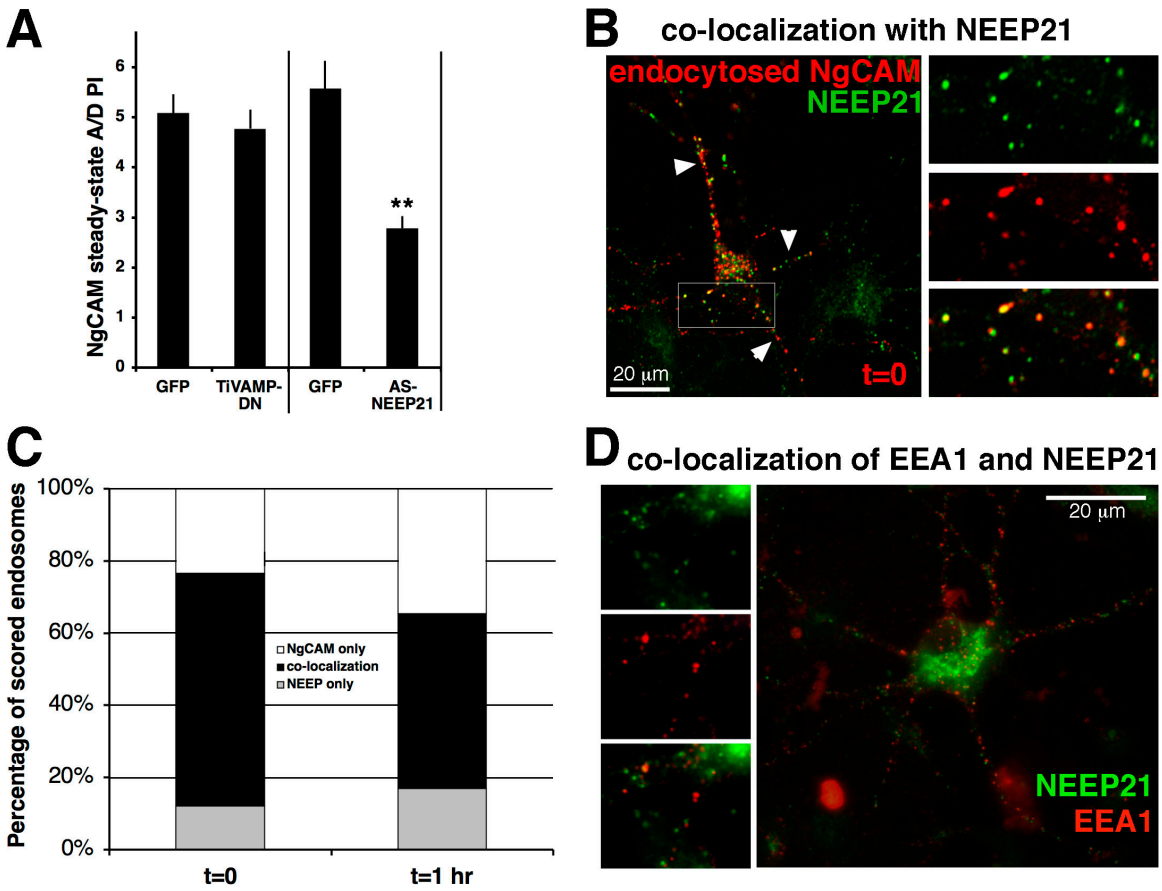

Figure 6. **Endocytosed NgCAM traverses the NEEP21-positive EE.** (A) Neurons were cotransfected with NgCAM and either dominant-negative Ti-VAMP (left) or anti-sense NEEP21 (right). GFP was expressed as a control. 18 h after transfection, surface NgCAM was detected with immunostaining. Coexpression of AS-NEEP21 but not Ti-VAMP-DN led to a significant decrease in the A/D PI (see Materials and methods). Error bars indicate SEM; **, statistical significance from GFP controls at $P < 0.001$. $n = 4$ independent experiments, scoring 20–25 cells per experiment for each condition. (B) NgCAM-expressing neurons were allowed to endocytose anti-NgCAM antibodies for 20 min before fixation. Endocytosed NgCAM was detected with a red secondary antibody, whereas endogenous NEEP21 was detected with a rabbit anti-NEEP21 antibody (green). Precise overlap of NgCAM and NEEP21 is observed (colocalization appears yellow). Single channels as well as overlaid channels are shown for the boxed area. A single confocal section is shown. Arrowheads indicate dendrites. (C) Extent of overlap was scored for cells loaded with anti-NgCAM antibodies for 20 min without a chase (left; t = 0) and after a 1-h chase (right; t = 60). Extent of overlap was binned into strong colocalization, NEEP only, and NgCAM only. NgCAM showed high colocalization (black) at t = 0, which diminished with time (right), whereas the no colocalization categories NEEP only and NgCAM only increased with time. (D) The EE populations enriched in EEA1 (red) or in NEEP21 (green) show poor colocalization. Single channel panels are shown on the left.

levels in AS-NEEP21–expressing cells, leading to saturation of the sorting machinery. We therefore compared the total mean surface intensity of NgCAM in cells expressing GFP as control or AS-NEEP21. No statistically significant differences in total surface NgCAM were observed (surface intensity in GFP = 5208 ± 832 arbitrary units; AS-NEEP21 = 5952 ± 534 arbitrary units). Because NEEP21 is found in the TGN as well as in endosomes (Steiner et al., 2002), either one could be the site of missorting. We therefore determined the A/D PI at steady state of a mutant NgCAM containing a point mutation in the somatodendritic sorting signal, NgCAM Y33A. This NgCAM mutant travels to the axon on a direct pathway from the TGN, bypassing somatodendritic endosomes (Wisco et al., 2003). The steady-state A/D PI of NgCAM Y33A was not reduced by coexpressing AS-NEEP21 (Fig. 7 A). Additionally, we determined the A/D PI of endosomally recycling NgCAM (using the same assays as for Fig. 3). The recycling A/D PI of NgCAM was also significantly diminished compared with control cells (Fig. 7 A, right). AS-NEEP21 therefore causes missorting of NgCAM during endosomal recycling.

NgCAM missorting occurs in the EE

We next asked whether the kinetics of endosomal trafficking of NgCAM were changed in AS-NEEP21–expressing cells. We predicted that endocytic uptake of NgCAM would be increased because higher levels of NgCAM are available for endocytosis on the somatodendritic surface at steady state in AS-NEEP21–expressing cells. We do in fact see more than twofold higher levels of endocytosed NgCAM in the soma at t = 0 in AS-NEEP21 compared with GFP controls (Fig. 7 B). For several other receptors, expression of AS-NEEP21 caused increased retention of the receptors in endosomes. We therefore compared the extent of NgCAM clearance from somatic endosomes at t = 40 min. Signal levels at t = 40′ were normalized to signal levels at t = 0 for each set because the initial signal levels were much higher for AS-NEEP21 to begin with (Fig. 7 C). We found a modest increase in NgCAM retention in AS-NEEP21–expressing cells ($P = 0.055$ by Mann Whitney *U* test).

In epithelial cells, cargo can leave the EE in three directions: direct local recycling to the plasma membrane, transport

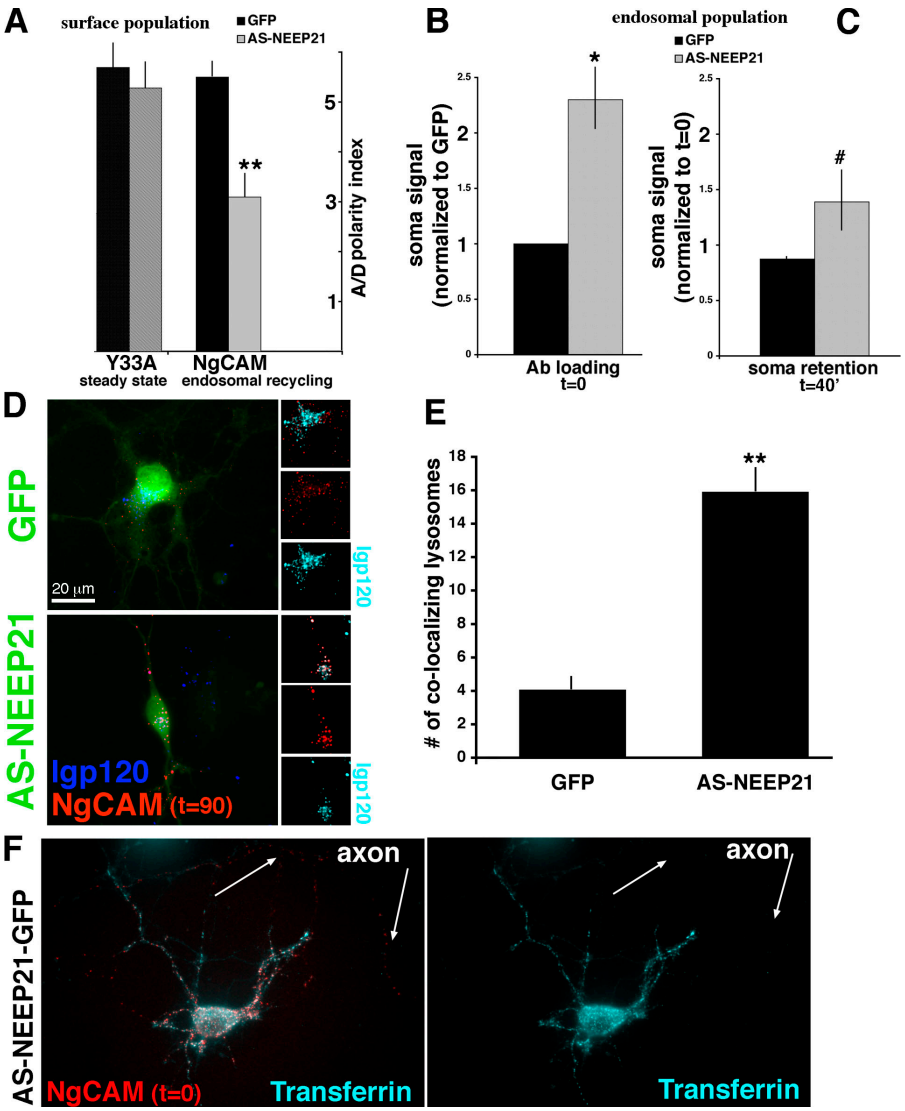

Figure 7. **Down-regulation of NEEP21 leads to missorting of endosomal NgCAM to the somatodendritic surface and to lysosomes.** (A) The A/D PI was determined for NgCAMY33A at steady state (left) and for NgCAM for endosomal recycling to the plasma membrane (t = 2.5 h; right) in cells coexpressing GFP as controls (black) or AS-NEEP21 (gray). Error bars indicate SEM; **, statistical significance from GFP controls at P < 0.001. *n* = 4 independent experiments scoring 12–17 cells per experiment for each condition. (B) The extent of anti-NgCAM antibody loading at t = 0 into somatic endosomes was quantified in control cells (black) or AS-NEEP-GFP coexpressing neurons (gray). Values were normalized to GFP-expressing control cells (Ab loading). (C) The presence of endocytosed NgCAM in somatic endosomes (soma retention) was quantitated at t = 0 and t = 40 min for cells coexpressing either GFP as control (black) or antisense NEEP21-GFP (AS-NEEP21; gray). Values were normalized to the t = 0 levels for each condition. *n* = 4 independent experiments, scoring 12–17 cells per experiment for each condition. Error bars indicate SEM. *, statistical significance from controls at P < 0.01; #, statistical significance from controls at P = 0.055 (Mann Whitney *U* test). (D) The extent of colocalization between the lysosomal lgp120 (blue) and endocytosed NgCAM (90-min chase; red) was visualized for cells coexpressing NgCAM and GFP (top) or NgCAM and AS-NEEP21-GFP (bottom). Single channel and merged images of the soma region are shown separately on the right. In these panels, lgp120 is displayed in aqua. Overlap with the red channel appears white. (E) Quantification of the number of colocalizing puncta from the experiment in D. *n* = 3 independent experiments scoring 12–17 cells per experiment and condition. Error bars indicate SEM; **, statistical significance from GFP controls at P < 0.001. (F) Localization of internalized Tf (aqua) and endocytosed NgCAM (red; 20-min load at t = 0) in cells coexpressing NgCAM and AS-NEEP21-GFP. The right panel shows the single channel for Tf. Although endocytosed NgCAM can be detected in endosomes along axons (red; left, arrows), no missorting of Tf (aqua) to the axon (arrows) is observed.

to the RE, or transport to the LE/lysosome (see Fig. 1 D). We next asked if the retention of endocytosed NgCAM in somatic endosomes (Fig. 7 C) might be, at least in part, caused by terminal missorting to LE/lysosomes. In control cells (Fig. 7 D, top), little overlap between NgCAM (red) and the lysosomal lgp120 (blue or aqua in insets) was observed (overlap appears white in the insets). AS-NEEP21–coexpressing cells, however, showed increased colocalization of endocytosed NgCAM with lgp120 (Fig. 7 D, bottom; and Fig. 7 E). NEEP21 function therefore biases the exit route from the EE such that NgCAM is preferentially transported to the RE rather than recycled to the somatodendritic surface or trafficked to lysosomes.

Lastly, we asked if Tf was missorted to the axon in AS-NEEP21–expressing cells. Such missorting would suggest that the somatodendritic EE could serve as a direct exit station toward the axon. No such missorting was observed and Tf remained somatodendritically restricted in antisense NEEP21–expressing cells (Fig. 7 F, aqua), whereas endocytosed NgCAM was additionally found in axonal endosomes (Fig. 7 F, red; arrows indicate axons).

Polarity of endogenous L1 is affected by down-regulation of NEEP21

We then asked if the axonal polarity of endogenous L1 was also dependent on NEEP21 function. We introduced the antisense NEEP21 plasmid by electroporation into dissociated hippocampal neurons before plating and then assayed the distribution of surface L1 at DIV3. Endogenous L1 was highly enriched on the axonal surface (Fig. 8 A, arrows) in GFP-expressing control cells (Fig. 8, A and A′, red) and little L1 was detected on the somatodendritic surface (arrowheads). When AS-NEEP21-GFP was expressed, L1 was readily detected on the axon (Fig. 8 B, arrows) but also on soma and dendrites (Fig. 8, B and B′, red, arrowheads). The A/D PI of endogenous L1 was significantly

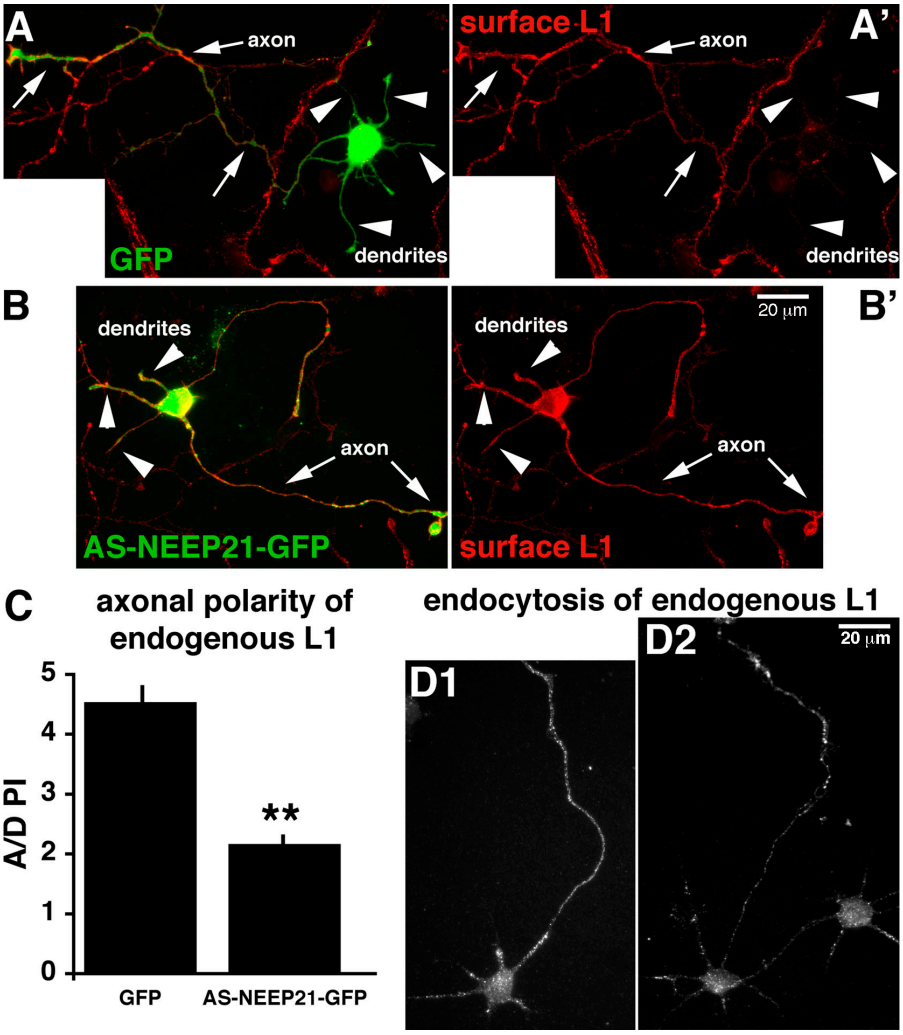

Figure 8. **Endogenous L1 mislocalizes to the somatodendritic domain when NEEP21 is down-regulated.** (A and B) Dissociated neurons were electroporated with GFP as control (A and A′) or AS-NEEP21-GFP (B and B′) and surface L1 was detected with a polyclonal anti-L1 antibody (red) at DIV3. In GFP-expressing control cells (A and A′), endogenous L1 is highly polarized to the axon (arrows) and only weakly found on dendrites (arrowheads). In AS-NEEP21-GFP–expressing cells (B and B′), endogenous L1 is additionally detected on the soma and dendrites. (C) The A/D PI was determined for endogenous surface L1 for control cells expressing GFP or AS-NEEP21-GFP. n = 50 cells for GFP; n = 63 cells for AS-NEEP21-GFP from two independent experiments. Error bars indicate SEM. **, statistical significance at $P < 0.0001$. (D) DIV3 neurons were incubated with polyclonal anti-L1 antibody for 20 min and then fixed and stained with secondary antibody after permeabilization. Labeled endosomes can be seen in axons, somata, and dendrites. Two examples are shown.

reduced in antisense NEEP21–expressing cells (Fig. 8 C). NEEP21 therefore promoted axonal polarization of endogenous L1 in young cultures. Because of two technical constraints, we were unable to assess the effects of AS-NEEP21 on endogenous L1 in mature cultures. (1) Endogenous L1 accumulates stably to high levels on the axonal surface. Introducing antisense NEEP21 at DIV8/9 (as we do for exogenously expressed NgCAM) made it impossible to detect the fate of the newly synthesized pool of L1 because such a large amount of endogenous L1 was already accumulated stably on the axonal surface at the time of transfection. (2) Mature cultures of DIV9–11 have a very dense network of criss-crossing axons. Trying to assess the polarity of endogenous L1 proved not to be possible because individual axons cannot be unambiguously traced to the cell body. Furthermore, axons commonly grow along dendrites, giving the erroneous impression that MAP2-positive processes are L1-positive.

The observation that endogenous L1 is sensitive to NEEP21 depletion suggested that a significant fraction of endogenous L1 also travels via somatodendritic endosomes to the axon. We therefore tested if endogenous L1 can be endocytosed in the somatodendritic domain by performing antibody uptake experiments in DIV3 neurons with an antibody against the endogenous L1. We observed extensive labeling of endosomes, both in axons and in the somatodendritic domain (Fig. 8, D1 and D2).

Live imaging of NEEP21-GFP and endocytosed NgCAM

Lastly, we determined if the NEEP21 compartment corresponded to the stationary NgCAM-containing endosomes or whether NEEP21 was also found in moving transport carriers together with NgCAM (Fig. 9 and Videos 6 and 7, available at http://www.jcb.org/cgi/content/full/jcb.200707143/DC1). Colocalization of endocytosed NgCAM and NEEP21-GFP was striking and precise (Fig. 9, A and C, yellow). These yellow compartments containing both NgCAM and NEEP21 were largely stationary (Fig. 9 A, asterisk), with only 2.5% of them moving (Fig. 9 C; n = 443). Unexpectedly, NEEP21-containing compartments did show frequent movements (Fig. 9 A, arrowheads) but the moving NEEP21 compartments rarely contained NgCAM. If only moving compartments were considered, 66% of them contained only NEEP21 (Fig. 9 D). Compartments containing NgCAM but not NEEP21 also moved (20.5%; Fig. 9 A, white arrows; and Fig. 9 C). The observed movements were episodic, frequently punctuated by pauses of many seconds (Fig. 9 B).

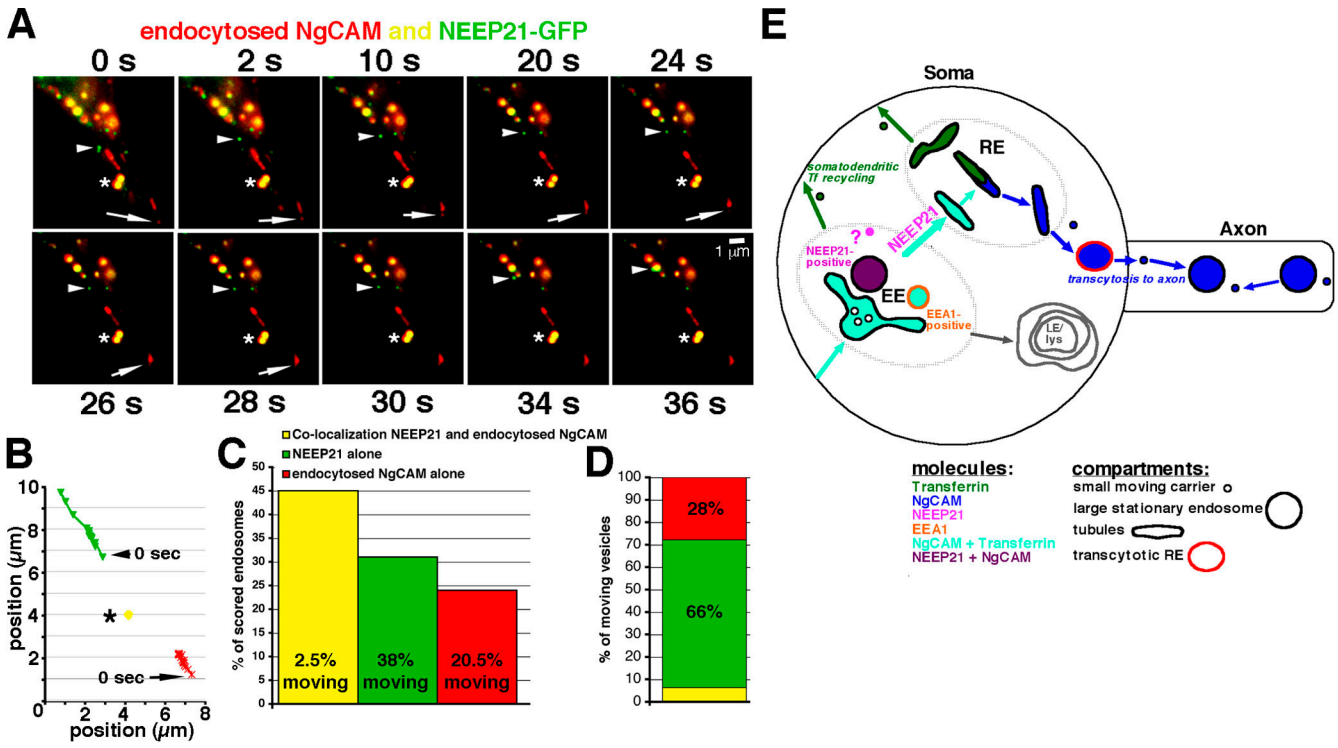

Figure 9. **Dynamic behavior of NEEP21-GFP and endocytosed NgCAM in endosomes.** (A and B) Live imaging of endocytosed NgCAM (red) and NEEP21-GFP (green). A portion of a proximal dendrite is shown (A). Images were captured every 2 s as indicated above each panel. Frames not shown displayed no movements. The trajectories for all twenty frames (0–38 s) are displayed in B for the three compartments marked by arrowheads, arrows, and asterisks in A. The starting point at 0 s is indicated. The NEEP21-containing and the NgCAM-containing compartments (marked with arrows/arrowheads) show movements, whereas the compartment containing both NEEP21 and endocytosed NgCAM (marked with an asterisk) does not move. See Video 6 (available at http://www.jcb.org/cgi/content/full/jcb.200707143/DC1). (C) Quantification of all scored endosomes (n = 443) in the 1-min imaging period. (D) Quantification of moving endosomes (n = 79; colors as defined in C). (E) Model of endosomal compartments involved in NgCAM transcytosis. Tf and NgCAM (aquamarine arrows) enter EEA1-positive EEs (orange) in the somatodendritic domain as well as NEEP21-positive EEs (purple), from where they are transported to the somatodendritic RE. Tf (green arrows) but not NgCAM (blue arrows) recycles to the somatodendritic surface from the EE and the RE. NgCAM (blue), however, sorts away from Tf into putative "transcytotic REs" (red) and travels anterogradely up the axon in small carriers. Large stationary endosomes along the axon (blue) accumulate endocytosed NgCAM and might provide intermediary stopover points into which motile carriers fuse and from which new motile carriers are generated. When NEEP21 is down-regulated by antisense, NgCAM is missorted, presumably in the NEEP21 endosome, toward the somatodendritic surface as well as to lysosomes (gray arrows; LE/lys). Tf, however, is not missorted to the axon.

We conclude that NgCAM accumulates in stationary NEEP21 endosomes and is transported in NEEP21-negative transport carriers. NEEP21-positive carriers are frequently observed but it is not known which cargo might be cotransported.

Discussion

NgCAM accumulates on the axonal plasma membrane via transcytosis, not via selective retrieval/retention

In this work, we tested two endocytosis-dependent models for axonal accumulation and show that NgCAM accumulates on the axon via transcytosis rather than via selective retrieval/retention. Based on previous kinetic experiments, we estimate that ~80% of NgCAM travels via transcytosis (Wisco et al., 2003). We propose the following model of the transcytotic pathway and the endosomal compartments involved (Fig. 9 E): NgCAM is taken up into somatodendritic EEA1-positive EEs. NgCAM traverses NEEP21-positive endosomes, from where it is preferentially trafficked to REs. Subsequently, endosomal NgCAM sorts away from Tf in the RE and is transported in tubules and small round carriers without Tf. Once NgCAM endosomal carriers enter the axon, many are transported by fast axonal transport. Large stationary endosomes along the axon accumulate endocytosed NgCAM and might provide intermediary stopover points into which motile carriers fuse and from which new motile carriers are generated. We propose that NEEP21 is required for faithful sorting of NgCAM to axons by facilitating trafficking from somatodendritic EEs to REs rather than local somatodendritic recycling or degradation. We conclude that functioning somatodendritic endosomes are required for axonal localization of NgCAM.

Live imaging of NgCAM-containing endosomes

We developed live imaging approaches to visualize the endosomal trafficking of NgCAM in cultured primary neurons. Trafficking of all NgCAM pools was shown previously by imaging NgCAM-GFP (Burack et al., 2000). To monitor endosomal but not post-TGN traffic, we labeled specifically endosomal pools of NgCAM by incubation with Alexa-labeled anti-NgCAM antibodies. In agreement with fixed samples, endocytosed NgCAM was found

prominently in somatodendritic endosomes. Most of the labeled endosomes were nonmobile, but small mobile transport carriers (either spherical or tubular) could be visualized in the soma and dendrites.

Endosomal transport in axons is thought to occur in a retrograde direction toward either somatic lysosomes or signaling endosomes (Parton et al., 1992). Anterograde fast axonal transport of endosomes is not usually observed. We show here directly by live imaging that NgCAM is transported anterogradely in endosomes in axons. The axonal NgCAM endosomes are reminiscent of compartments revealed by live imaging of syntaxin13-GFP in cultured neurons (Prekeris et al., 1999). Fast axonal anterograde transport of endosomes might thus serve to redistribute a distinct set of membrane proteins from the dendrite to axons. Other cargos (such as the type 1 cannabinoid receptor; Leterrier et al., 2006) might require some of the same compartments as NgCAM.

Identity of somatodendritic compartments containing NgCAM

Endocytosed NgCAM is initially but transiently found with EEA1 and Tf in EEs. It is subsequently found in compartments that are closely apposed to Tf-containing REs. We suggest, based on confocal images of fixed cells and on dual live imaging, that NgCAM progressively sorts away from Tf into mobile tubules and small spherical carriers. These NgCAM-containing carriers might fuse with intermediate compartments before entering the axon. It remains to be determined if the REs found at and within dendritic spines (Park et al., 2006) are accessible to recycling NgCAM as well or constitute a discrete subset. By immuno-EM, we observed a preponderance of endocytosed NgCAM in MVBs in the soma. Although many of these MVBs are likely to be predegradative and degradative compartments, it remains to be determined if NgCAM-containing MVBs are intermediates on the transcytotic pathway.

In MDCK cells, all transcytosing cargo traverses the RE (Sheff et al., 1999). Our data similarly suggest that transcytosis to the axon does not occur directly from the EE but from the RE. It additionally suggests that trafficking from REs toward either the axon or the somatodendritic surface is mediated by distinct signals in the cargo proteins. Whether or not sequences in the cytoplasmic tail of NgCAM mediate sorting to the axon from somatodendritic endosomes remains to be determined.

Our studies provide insights into the dynamics and organization of neuronal endosomes by using dual live imaging of two differentially sorted recycling cargos. In cultured neurons, no singular, perinuclear RE was observed. (de Marco et al., 2006; Thompson et al., 2007). Rather, NgCAM-containing endosomes were dispersed throughout the soma at all times of chase. Similar to endosomes in nonneuronal cells (Mukherjee and Maxfield, 2000), lipid composition appears to be mosaic in neuronal endosomes as well, such that NgCAM endosomes accumulate, whereas Tf endosomes exclude DiI. Our observations are consistent with lateral segregation of Tf and NgCAM in single endosomes but only ultrastructural studies ultimately have the resolution to prove this point.

NEEP21 function in the transcytotic pathway

NEEP21 was initially identified as an interacting partner of the endosomal syntaxin13 (Steiner et al., 2002). NEEP21 plays crucial roles in regulating recycling of multiple cargos (Steiner et al., 2002, 2005; Debaigt et al., 2004; Alberi et al., 2005). Endocytosed NgCAM colocalizes precisely with NEEP21 in cultured hippocampal neurons and exits with slow kinetics. The NEEP21 endosomes might therefore serve as a "warehouse" not only for synaptic AMPA receptors but also for transcytosing NgCAM. Furthermore, down-regulation of NEEP21 affects sorting of NgCAM. The NEEP21 compartment therefore is functionally on the pathway of endosomal NgCAM trafficking toward the axon. Importantly, endogenous L1 is also affected by down-regulation of NEEP21, which argues that transcytosis is a relevant pathway for L1 in young neurons. Interestingly, NEEP21 and syntaxin13 are highly expressed during development but down-regulated in adulthood (Hirling et al., 2000; Steiner et al., 2002). Therefore, the trafficking pathways of receptors might be developmentally regulated. Our work provides new insights into the dynamics and organization of neuronal endosomes and indicates the importance of neuronal endosomes in the polarized membrane traffic to axons.

Materials and methods

Cell culture and reagents

Primary cultures of hippocampal neurons were grown as described previously (Wisco et al., 2003) and cultured for 8–16 d. The 8D9 anti-NgCAM hybridoma was obtained from the National Institutes of Health Hybridoma Bank. Tissue culture supernatants were concentrated over a T-gel column (Thermo Fisher Scientific). Purified IgGs were coupled to Alexa-488 according to manufacturer's instructions (Invitrogen). 8D9 Fab fragments were prepared using the Fab preparation kit according to manufacturer's instructions (Thermo Fisher Scientific). Rabbit anti-EEA1 antibody was obtained from Chemicon and Texas red–rat Tf was obtained from Jackson ImmunoResearch Laboratories. Polyclonal antibodies raised against NEEP21 and plasmid AS-NEEP2-GFP were previously described by Steiner et al. (2002). Anti-lgp120 rabbit antiserum "Mingus" was a gift from I. Mellman (Yale University, New Haven, CT). Anti-L1 rabbit serum was provided by V. Lemmon (University of Miami, Miami, FL). Secondary reagents were obtained from Invitrogen except anti–mouse Fab-specific FITC, which was obtained from Sigma-Aldrich. Human L1-myc was provided by D. Benson (Mount Sinai School of Medicine, New York, NY), and rat L1-myc was provided by D. Felsenfeld (Mount Sinai School of Medicine). Ti-VAMP reagents were provided by T. Galli (Institut National de la Santé et de la Recherche Médicale, Paris, France). NgCAM cDNA was subcloned into pCB6 with the Bluescript multiple cloning site containing a nonenhanced cytomegalovirus promoter. NgCAM Y33A has been described previously (Wisco et al., 2003).

Transfections and infections

Neuronal cultures at DIV9–12 were transfected using Lipofectamine 2000 with 1 µg DNA and 3 µl Lipofectamine 2000 (Invitrogen) for 60–90 min, washed, and incubated for 16–20 h. To reduce the number of overexpressing cells, the NgCAM plasmid was mixed with an empty plasmid containing no insert. For some experiments, an NgCAM adenovirus was used as described previously (Wisco et al., 2003).

Down-regulation of NEEP21 and Ti-VAMP

To test if NEEP21 was functionally important for trafficking of NgCAM to the axon, we used the same anti-sense strategy that has previously been used successfully (Steiner et al., 2002). For these experiments, neurons were transfected simultaneously with antisense NEEP21-GFP and NgCAM plasmids; control cells were transfected with GFP and NgCAM plasmids. In order to quantify the extent of downregulation by AS-NEEP21 expression, the endogenous NEEP21 staining in the soma of individual cells (n = 23 for each of the AS-NEEP21–transfected cells or untransfected control cells) was determined using Image J. NEEP21 showed a mean reduction of ~50%

due to antisense expression. For Ti-VAMP, a dominant-negative construct containing the longin domain of Ti-VAMP was used. This construct leads to inhibition of neurite outgrowth (Martinez-Arca et al., 2001) and delay of L1 recycling from PC12 cells (Alberts et al., 2003). Ti-VAMP longin, in our hands, also had a profound inhibitory effect on axon outgrowth of hippocampal neurons, showing that it was active as a dominant-negative.

Microscopy and live imaging

For live imaging, cells were grown on large round coverslips (Bellco Biotechnology) or glass-bottom dishes (MatTek). Cells were transfected with NgCAM plasmid 18 h before imaging and incubated with Alexa 488–coupled 8D9 anti-NgCAM antibody for 20–60 min, washed, and mounted in a live imaging chamber on a heated stage under 5% CO_2. To visualize axonal NgCAM-containing endosomes, cells were acid stripped (see next paragraph) and washed before imaging. Live imaging was performed on a microscope (Axiovert; Carl Zeiss, Inc.) using a 63× Plan Apo lens (Carl Zeiss, Inc.) and a camera (Orca ER; Hamamatsu). Openlab software was used for image capture at exposures of 80–150 ms with 2× binning. For some experiments, imaging was performed on an IX81 microscope (Olympus) using a 100× oil immersion objective and captured with 100 ms exposures and 1× binning. For dual imaging of endocytosed NgCAM and NEEP21-GFP, cells were transfected with NgCAM and NEEP21-GFP plasmids and uptake was performed with an Alexa 568–antiNgCAM antibody. Only cells expressing low to moderate amounts of NEEP21-GFP were chosen for imaging to minimize overexpression artifacts. Confocal imaging was performed on a laser scanning microscope (LSM 510; Carl Zeiss, Inc.) with a 63× 1.4 differential interference contrast microscopy oil Plan Apochromat objective or on a UV confocal laser scanning microscope (TCS-SP1; Leica) equipped with a four-channel spectrophotometer scan head and four lasers (350 nm Ar-UV, 488 nm argon, 568 nm krypton, and 633 nm HeNe). A 63× 1.4 NA Plan Apo objective lens was used.

Endocytosis assay with acid strip

Neurons expressing NgCAM for 18 h were incubated with 8D9 anti-NgCAM antibodies for 20 min at 37°C and washed several times; all antibody remaining on the surface was then stripped by treatment with MEM, pH 2, for 2 min (Fourgeaud et al., 2003), washed extensively, and returned to the incubator for various amounts of times before fixation in 2% paraformaldehyde/3% sucrose/PBS, pH 7.4. Recycled 8D9 antibody was detected before permeabilization with Alexa 647 or Cy5 secondary goat anti–mouse antibody. Because all remaining primary antibodies had been removed from the surface by acid stripping before the chase period, any surface-associated Alexa 647 fluorescence at later chase times was caused by the reappearance of previously internalized anti-NgCAM primary antibodies. Internalized NgCAM antibody was detected by applying Alexa-568 goat anti–mouse antibody after permeabilization. Permeabilization was achieved either with 0.05% saponin or 0.2% Triton X-100 for 10 min at room temperature as described previously (Wisco et al., 2003). The uptake of lipophilic dye (DiIC18[5]-DS; Invitrogen) in neurons was conducted as described by Manderson et al. (2007).

Immunogold EM

Immunogold EM of ultrathin cryosections was performed according to the flat-embedding technique described previously (Oorschot et al., 2002). Cells were fixed in 2% paraformaldehyde and 0.2% glutaraldehyde in 0.1 M PHEM buffer (60 mM Pipes, 25 mM Hepes, 10 mM EGTA, and 2 mM $MgCl_2$, pH 6.9) for 2 h at room temperature after an endocytosis assay. After rinsing first in PBS with 0.02% M glycine and then in PBS with 0.1% BSA, the fixed cell monolayer was directly embedded in a thin layer of 12% gelatin phosphate buffer, which was prewarmed to 37°C. The gelatin was solidified at 4°C and subjected to a prolonged infiltration with 2.3 M sucrose for 48 h at 4°C on a rocker. Coverslips were gently removed from the gelatin layer now containing some cells transferred from the coverslip. Approximately 1 mm^3 blocks of selected areas with cells were cut off from the gelatin layer, mounted on aluminum pins in a way that the gelatin-embedded cells were orientated upwards, and then frozen in liquid nitrogen. Ultrathin cryosections parallel to the gelatin-embedded cell monolayer were cut at −120°C in a cryo ultramicrotome (Diatome) and picked up in a 1:1 mixture of 2.3 M sucrose and 2% methylcellulose and immunolabeled according to the protein A–gold method.

AS-NEEP21 expression in young neurons

Nucleofection of freshly dissociated neurons was performed using a Nucleofector device (Amaxa Biosystems) according to the manufacturer's instructions. At DIV3 after nucleofection, neurons were surface-labeled live with anti–rat L1 and fixed with 2% paraformaldehyde, followed by secondary antibody labeling. For visualizing endocytosed L1, endocytosis assay with acid strip was applied.

Image quantification

The same adjustments were performed on all images equally for each set of quantifications. *t* tests were performed using Statistics software 13 (SPSS).

Endocytosis pulse/chase experiments (Fig. 2). Total soma fluorescence was determined using Image J after background subtraction. The soma was outlined using the freehand tracing function and total fluorescence was measured in the outlined region of interest. Measurements were taken for 15–20 cells per experiment and condition.

Endosome intensity (Fig. 2 D). A one-pixel-wide line was traced along axons and dendrites in Image J and plotted as an intensity profile. The maximal intensity of the peaks in the trace, which correspond to NgCAM-containing endosomes, were measured and averaged from 10 axons and 10 dendrites each for four experiments.

A/D PI (Figs. 2 and 9). Axon and dendrite fluorescence intensities were measured along a one-pixel-wide line in Image J after background subtraction and normalized to length. A/D PI was obtained by dividing the mean axon intensity by the mean dendrite intensity.

Colocalization of endocytosed NgCAM and markers of endosomal compartments (Figs. 5 and 8). When quantifying the extent of colocalization, we found that the relative intensities of the two markers under study often differed over a wide range, from roughly equal intensities to 10–20-fold higher intensity of one marker compared with the other. To reflect this observation, colocalization was scored as being either "none" (>25-fold higher intensity of one marker compared with the other), "high" (intensity ratios of the two markers between 1 and 5), or "low" (intensity ratios of the two markers between 5 and 25). Black levels of images were adjusted to drop out nonspecific background using Photoshop (Adobe). The cursor was centered on all identifiable endosomal puncta and the red and green levels were recorded. The ratio of red/green was then determined and binned into five bins such that the ratio of intensities for the two channels was in the range of 1–5 (high colocalization), 5–25 (low colocalization), and >25 (no colocalization). In Fig. 8, high colocalization and low colocalization bins were combined into a single bin because the low colocalization bins were small and did not change with chase time.

Colocalization with lysosomes (Fig. 9). The number of puncta containing strong signals of both lgp120 and endocytosed NgCAM was counted in the soma region of 12–17 cells per experiment and condition.

Online supplemental material

Fig. S1 shows detectability of endocytosed NgCAM in somatodendritic endosomes. Fig. S2 shows a single-frame display of Fig. 4 D. Fig. S3 shows that the lipophilic dye DiIC18(5)DS preferentially labels NgCAM-containing endosomes. Video 1 shows the dynamic behavior of NgCAM-containing endosomes in the soma of a DIV10 cultured hippocampal neuron. Video 2 shows the dynamics of NgCAM-containing endosomes in the axon of a DIV10 cultured hippocampal neuron. Video 3 shows dual live imaging of two endosomal cargos in proximal dendrites. Video 4 is a high-contrast, cropped movie showing long distance movement of a small NgCAM-positive endosomal carrier in a dendrite. Video 5 is a high-contrast, cropped movie showing coordinated movement of a small endosomal carrier containing laterally segregated cargos in the soma. Video 6 shows dual live imaging of NEEP21-GFP and endocytosed NgCAM in a proximal dendrite. Video 7 shows a second example of dual live imaging of NEEP21-GFP and endocytosed NgCAM in a proximal dendrite. Online supplemental materials is available at available at http://www.jcb.org/cgi/content/full/jcb.200707143/DC1.

Crucial reagents were generously provided by Drs. Deanna Benson and Dan Felsenfeld, Thierry Galli, Ira Mellman, and Vance Lemmon. Special thanks go to Drs. George Bloom and Ed Perez-Reyes for help and access to their live-imaging rigs. We thank Drs. George Bloom, Kevin Pfister, and Frank Solomon for comments on the manuscript. We thank the members of the Winckler Laboratory Julie Lim and Chad Lane for technical help with the experiments and Max Vakulenko for insightful discussions.

This work was supported by the National Institutes of Health/National Institute of Neurological Disorders and Stroke (grant 1RO1NS 045969-06 to B. Winckler), a Basil O'Connor grant from the March of Dimes Foundation (FY01-517 to B. Winckler), and the Swiss National Science Foundation (grant 3100A0-111935/1 to H. Hirling). P. Kujala was supported by grant ALW8PJ/00-31 from the Research Council for Earth and Life Sciences (Nederlandse Organisatie voor Wetenschappelijk Onderzoek-Aard en Levens Wetenschappen) to J. Klumperman.

Submitted: 20 July 2007
Accepted: 28 January 2008

References

Alberi, S., B. Boda, P. Steiner, I. Nikonenko, H. Hirling, and D. Muller. 2005. The endosomal protein NEEP21 regulates AMPA receptor-mediated synaptic transmission and plasticity in the hippocampus. *Mol. Cell. Neurosci.* 29:313–319.

Alberts, P., and T. Galli. 2003. The cell outgrowth secretory endosome (COSE): a specialized compartment involved in neuronal morphogenesis. *Biol. Cell.* 95:419–424.

Alberts, P., R. Rudge, I. Hinners, A. Muzerelle, S. Martinez-Arca, T. Irinopoulou, V. Marthiens, S. Tooze, F. Rathjen, P. Gaspar, and T. Galli. 2003. Cross talk between tetanus neurotoxin-insensitive vesicle-associated membrane protein-mediated transport and L1-mediated adhesion. *Mol. Biol. Cell.* 14:4207–4220.

Boiko, T., M. Vakulenko, H. Ewers, C.C. Yap, C. Norden, and B. Winckler. 2007. Ankyrin-dependent and -independent mechanisms orchestrate axonal compartmentalization of L1 family members neurofascin and L1/neuroglia cell adhesion molecule. *J. Neurosci.* 27:590–603.

Brown, T.C., I.C. Tran, D.S. Backos, and J.A. Esteban. 2005. NMDA receptor-dependent activation of the small GTPase Rab5 drives the removal of synaptic AMPA receptors during hippocampal LTD. *Neuron.* 45:81–94.

Burack, M.A., M.A. Silverman, and G. Banker. 2000. The role of selective transport in neuronal protein sorting. *Neuron.* 26:465–472.

Chang, M.C., D. Wisco, H. Ewers, C. Norden, and B. Winckler. 2006. Inhibition of sphingolipid synthesis affects kinetics but not fidelity of L1/NgCAM transport along direct but not transcytotic axonal pathways. *Mol. Cell. Neurosci.* 31:525–538.

Cremona, O., and P. De Camilli. 1997. Synaptic vesicle endocytosis. *Curr. Opin. Neurobiol.* 7:323–330.

de Marco, M.C., R. Puertollano, J.A. Martinez-Menarguez, and M.A. Alonso. 2006. Dynamics of MAL2 during glycosylphosphatidylinositol-anchored protein transcytotic transport to the apical surface of hepatoma HepG2 cells. *Traffic.* 7:61–73.

Debaigt, C., H. Hirling, P. Steiner, J.P. Vincent, and J. Mazella. 2004. Crucial role of neuron-enriched endosomal protein of 21 kDa in sorting between degradation and recycling of internalized G-protein-coupled receptors. *J. Biol. Chem.* 279:35687–35691.

Deinhardt, K., and G. Schiavo. 2005. Endocytosis and retrograde axonal traffic in motor neurons. *Biochem. Soc. Symp.* 72:139–150.

Deinhardt, K., S. Salinas, C. Verastegui, R. Watson, D. Worth, S. Hanrahan, C. Bucci, and G. Schiavo. 2006. Rab5 and Rab7 control endocytic sorting along the axonal retrograde transport pathway. *Neuron.* 52:293–305.

Fache, M.P., A. Moussif, F. Fernandes, P. Giraud, J.J. Garrido, and B. Dargent. 2004. Endocytotic elimination and domain-selective tethering constitute a potential mechanism of protein segregation at the axonal initial segment. *J. Cell Biol.* 166:571–578.

Fourgeaud, L., A.S. Bessis, F. Rossignol, J.P. Pin, J.C. Olivo-Marin, and A. Hemar. 2003. The metabotropic glutamate receptor mGluR5 is endocytosed by a clathrin-independent pathway. *J. Biol. Chem.* 278:12222–12230.

Garrido, J.J., F. Fernandes, P. Giraud, I. Mouret, E. Pasqualini, M.P. Fache, F. Jullien, and B. Dargent. 2001. Identification of an axonal determinant in the C-terminus of the sodium channel Na(v)1.2. *EMBO J.* 20:5950–5961.

Garrido, J.J., F. Fernandes, A. Moussif, M.P. Fache, P. Giraud, and B. Dargent. 2003. Dynamic compartmentalization of the voltage-gated sodium channels in axons. *Biol. Cell.* 95:437–445.

Hemar, A., J.C. Olivo, E. Williamson, R. Saffrich, and C.G. Dotti. 1997. Dendroaxonal transcytosis of transferrin in cultured hippocampal and sympathetic neurons. *J. Neurosci.* 17:9026–9034.

Hirling, H., P. Steiner, C. Chaperon, R. Marsault, R. Regazzi, and S. Catsicas. 2000. Syntaxin 13 is a developmentally regulated SNARE involved in neurite outgrowth and endosomal trafficking. *Eur. J. Neurosci.* 12:1913–1923.

Howe, C.L., and W.C. Mobley. 2004. Signaling endosome hypothesis: A cellular mechanism for long distance communication. *J. Neurobiol.* 58:207–216.

Kamiguchi, H., and V. Lemmon. 1998. A neuronal form of the cell adhesion molecule L1 contains a tyrosine-based signal required for sorting to the axonal growth cone. *J. Neurosci.* 18:3749–3756.

Kamiguchi, H., and V. Lemmon. 2000. Recycling of the cell adhesion molecule L1 in axonal growth cones. *J. Neurosci.* 20:3676–3686.

Kennedy, M.J., and M.D. Ehlers. 2006. Organelles and trafficking machinery for postsynaptic plasticity. *Annu. Rev. Neurosci.* 29:325–362.

Kulangara, K., M. Kropf, L. Glauser, S. Magnin, S. Alberi, A. Yersin, and H. Hirling. 2007. Phosphorylation of glutamate receptor interacting protein 1 regulates surface expression of glutamate receptors. *J. Biol. Chem.* 282:2395–2404.

Lai, H.C., and L.Y. Jan. 2006. The distribution and targeting of neuronal voltage-gated ion channels. *Nat. Rev. Neurosci.* 7:548–562.

Leterrier, C., J. Laine, M. Darmon, H. Boudin, J. Rossier, and Z. Lenkei. 2006. Constitutive activation drives compartment-selective endocytosis and axonal targeting of type 1 cannabinoid receptors. *J. Neurosci.* 26:3141–3153.

Manderson, A.P., J.G. Kay, L.A. Hammond, D.L. Brown, and J.L. Stow. 2007. Subcompartments of the macrophage recycling endosome direct the differential secretion of IL-6 and TNFα. *J. Cell Biol.* 178:57–69.

Martinez-Arca, S., S. Coco, G. Mainguy, U. Schenk, P. Alberts, P. Bouille, M. Mezzina, A. Prochiantz, M. Matteoli, D. Louvard, and T. Galli. 2001. A common exocytotic mechanism mediates axonal and dendritic outgrowth. *J. Neurosci.* 21:3830.

Maxfield, F.R., and T.E. McGraw. 2004. Endocytic recycling. *Nat. Rev. Mol. Cell Biol.* 5:121–132.

Mukherjee, S., and F.R. Maxfield. 2000. Role of membrane organization and membrane domains in endocytic lipid trafficking. *Traffic.* 1:203–211.

Oorschot, V., H. de Wit, W.G. Annaert, and J. Klumperman. 2002. A novel flat-embedding method to prepare ultrathin cryosections from cultured cells in their in situ orientation. *J. Histochem. Cytochem.* 50:1067–1080.

Overly, C.C., and P.J. Hollenbeck. 1996. Dynamic organization of endocytic pathways in axons of cultured sympathetic neurons. *J. Neurosci.* 16:6056–6064.

Park, M., E.C. Penick, J.G. Edwards, J.A. Kauer, and M.D. Ehlers. 2004. Recycling endosomes supply AMPA receptors for LTP. *Science*. 305:1972–1975.

Park, M., J.M. Salgado, L. Ostroff, T.D. Helton, C.G. Robinson, K.M. Harris, and M.D. Ehlers. 2006. Plasticity-induced growth of dendritic spines by exocytic trafficking from recycling endosomes. *Neuron.* 52:817–830.

Parton, R.G., K. Simons, and C.G. Dotti. 1992. Axonal and dendritic endocytic pathways in cultured neurons. *J. Cell Biol.* 119:123–137.

Peden, A.A., V. Oorschot, B.A. Hesser, C.D. Austin, R.H. Scheller, and J. Klumperman. 2004. Localization of the AP-3 adaptor complex defines a novel endosomal exit site for lysosomal membrane proteins. *J. Cell Biol.* 164:1065–1076.

Prekeris, R., D.L. Foletti, and R.H. Scheller. 1999. Dynamics of tubulovesicular recycling endosomes in hippocampal neurons. *J. Neurosci.* 19:10324–10337.

Sachse, M., G. Ramm, G. Strous, and J. Klumperman. 2002. Endosomes: multipurpose designs for integrating housekeeping and specialized tasks. *Histochem. Cell Biol.* 117:91–104.

Sampo, B., S. Kaech, S. Kunz, and G. Banker. 2003. Two distinct mechanisms target membrane proteins to the axonal surface. *Neuron.* 37:611–624.

Schmid, S.L., and E. Smythe. 1991. Stage-specific assays for coated pit formation and coated vesicle budding in vitro. *J. Cell Biol.* 114:869–880.

Schmidt, M.R., and V. Haucke. 2007. Recycling endosomes in neuronal membrane traffic. *Biol. Cell.* 99:333–342.

Schweizer, F.E., and T.A. Ryan. 2006. The synaptic vesicle: cycle of exocytosis and endocytosis. *Curr. Opin. Neurobiol.* 16:298–304.

Segal, R.A. 2003. Selectivity in neurotrophin signaling: theme and variations. *Annu. Rev. Neurosci.* 26:299–330.

Sheff, D.R., E.A. Daro, M. Hull, and I. Mellman. 1999. The receptor recycling pathway contains two distinct populations of early endosomes with different sorting functions. *J. Cell Biol.* 145:123–139.

Slepnev, V.I., and P. De Camilli. 2000. Accessory factors in clathrin-dependent synaptic vesicle endocytosis. *Nat. Rev. Neurosci.* 1:161–172.

Sonnichsen, B., S. De Renzis, E. Nielsen, J. Rietdorf, and M. Zerial. 2000. Distinct membrane domains on endosomes in the recycling pathway visualized by multicolor imaging of Rab4, Rab5, and Rab11. *J. Cell Biol.* 149:901–914.

Steiner, P., J.C. Sarria, L. Glauser, S. Magnin, S. Catsicas, and H. Hirling. 2002. Modulation of receptor cycling by neuron-enriched endosomal protein of 21 kD. *J. Cell Biol.* 157:1197–1209.

Steiner, P., S. Alberi, K. Kulangara, A. Yersin, J.C. Sarria, E. Regulier, S. Kasas, G. Dietler, D. Muller, S. Catsicas, and H. Hirling. 2005. Interactions between NEEP21, GRIP1 and GluR2 regulate sorting and recycling of the glutamate receptor subunit GluR2. *EMBO J.* 24:2873–2884.

Sudhof, T.C. 2004. The synaptic vesicle cycle. *Annu. Rev. Neurosci.* 27:509–547.

Susalka, S.J., and K.K. Pfister. 2000. Cytoplasmic dynein subunit heterogeneity: implications for axonal transport. *J. Neurocytol.* 29:819–829.

Thompson, A., R. Nessler, D. Wisco, E. Anderson, B. Winckler, and D. Sheff. 2007. Recycling endosomes of polarized epithelial cells actively sort apical and basolateral cargos into separate subdomains. *Mol. Biol. Cell.* 18:2687–2697.

von Bartheld, C.S. 2004. Axonal transport and neuronal transcytosis of trophic factors, tracers, and pathogens. *J. Neurobiol.* 58:295–314.

Winckler, B. 2004. Pathways for axonal targeting of membrane proteins. *Biol. Cell.* 96:669–674.

Wisco, D., E.D. Anderson, M.C. Chang, C. Norden, T. Boiko, H. Folsch, and B. Winckler. 2003. Uncovering multiple axonal targeting pathways in hippocampal neurons. *J. Cell Biol.* 162:1317–1328.

Xu, J., Y. Zhu, and S.F. Heinemann. 2006. Identification of sequence motifs that target neuronal nicotinic receptors to dendrites and axons. *J. Neurosci.* 26:9780–9793.